



**Linking sedimentation rates and large-scale architecture for
facies prediction in non-marine basins. (Paleogene,
Almazán Basin, Spain)**

Journal:	<i>Basin Research</i>
Manuscript ID:	BRE-120-2014.R1
Manuscript Type:	Original Article
Date Submitted by the Author:	n/a
Complete List of Authors:	VALERO, LUIS; University of Barcelona, Stratigraphy, Paleontology and Marine Geosciences Huerta, Pedro; University of Salamanca, Geology Garcés, Miguel; University of Barcelona, Stratigraphy, Paleontology and Marine Geosciences Armenteros, Ildefonso; University of Salamanca, Geology Beamud, Elisabet; ICTJA, Laboratori de Paleomagnetisme Gómez-Paccard, Miriam; ICTJA,
Keywords:	tectonics and sedimentation, stratigraphy, sedimentology, sequence stratigraphy, magnetostratigraphy

SCHOLARONE™
Manuscripts

Linking sedimentation rates and large-scale architecture for facies prediction in non-marine basins. (Paleogene, Almazán Basin, Spain)

Valero L.¹, Huerta P.², Garcés M.¹, Armenteros, I.³, Beamud, E.⁴, Gómez-Paccard, M.⁵

1: Dept. d'Estratigrafia, Paleontologia i Geociències Marines, Facultat de Geologia, Universitat de Barcelona, 08028, Barcelona, Spain

2: Dept. Geología, Universidad de Salamanca, Escuela Politécnica Superior de Ávila, 05003-Ávila, Spain 3: Dept. Geología, Universidad de Salamanca, Facultad de Ciencias 37071-Salamanca, Spain

4: Laboratori de Paleomagnetisme CCI-TUB-ICTJA CSIC, 08028- Barcelona, Spain

5: Géosciences-Rennes, UMR 6118, Université de Rennes 1, Campus de Beaulieu, Bât. 6 15, CS 74205, 35042 Rennes, France.

0.- ABSTRACT

This paper focuses on the relationships between the large-scale stratigraphic architecture of the Almazán basin infill and the sedimentation rates (SR) calculated for precise time intervals. Our aim is to improve the understanding of the timing and causes of the architectural changes, their significance in terms of accommodation space and sediment supply, and their relationship with climate and tectonics. The study area includes the Gómara fluvial fan, the main sediment transfer system of the Almazán basin during Paleogene times. Its large-scale architecture shifted through time between a stacking pattern of low density ribbon-like and high density sheet-like channel fills. Laterally to the fluvial system, mudstone and evaporitic mudstone units represented evaporitic mudflats which passed laterally into palustrine/lacustrine limestone units interpreted as lakes and ponds. Stacked calcretes occurred in distal alluvial and distal floodplain settings. A magnetostratigraphy encompassing 2600 meters guided by available fossil mammal biochronology has provided a temporal framework that spans the complete Paleogene infill of the basin, from Late Lutetian to Late Oligocene, filling a gap in the Cenozoic chronostratigraphy of Spanish basins. This permits to constrain the kinematics of the structures both in the basin and in its margins, and to provide the timing for the depositional sequences. These data, combined with a magnetostratigraphic map, where magnetic reversals were traced through the Gómara monocline, allow a detailed analysis of the SR variability across the fluvial system and its adjacent depositional environments. The results show that high sedimentation rates (around 30-40 cm/kyr) are related to fluvial environments with low density ribbon-shaped channels, while low SR (around or below 10 cm/kyr) are related to high density sheet-like channels. Laterally, mud dominated environments with high SR (15-20 cm/kyr) grade into palustrine/lacustrine carbonated environments with low SR (around 9 cm/kyr). The lowest SR (about 3 cm/kyr) are related to the development of stacked calcrete profiles in distal floodplain and in the connection of distal alluvial and palustrine/lacustrine units.

1.- INTRODUCTION

1
2
3 The development of sequence stratigraphy has provided a framework for basin-wide
4 correlations, interpretation and prediction of sedimentary facies and environments
5 (Mitchum *et al.*, 1977; Vail & Mitchum, 1977; Posamentier, 1988; Van Wagoner *et al.*,
6 1988; Catuneanu, 2006). A large number of studies have focused on the variations of
7 large-scale architecture of fluvial systems in order to understand why, where and
8 when highly interconnected fluvial channels occur (Bridge & Leeder, 1979; Shanley &
9 McCabe, 1991; Wright & Marriott, 1993; Mackey & Bridge, 1995; Legarreta & Uliana,
10 1998; Sheets *et al.*, 2002; Hickson *et al.*, 2005).

11
12
13 The architectural arrangement of the sedimentary record in non-marine basins is the
14 response to the interplay between accommodation space and sediment supply
15 (Catuneanu *et al.*, 2009). The main allogenic factors driving changes in accommodation
16 space and sediment supply are tectonics and climate, which also modify the slope of
17 the system (Catuneanu & Elango, 2001), the avulsion rate (Bryant *et al.*, 1995; Heller &
18 Paola, 1996), the bypass ratio, and the amount of sediment extracted along the
19 sediment transport system (Strong *et al.*, 2005; Paola & Martin, 2012; Michael *et al.*,
20 2014). Here, we hypothesize that the characterization of the large-scale architectural
21 arrangement together with quantification of sedimentary rates can help assessing the
22 relative role of accommodation and sediment supply in basin infill history.
23
24

25
26 Understanding the main controls on the occurrence of highly interconnected sheet like
27 channels is highly important for oil industry, groundwater exploration, and for CO₂
28 storage in non-marine basins because it could help reservoir prediction (Huerta *et al.*,
29 2011). This paper is focused on the calculation of sedimentation rates and the
30 subsequent comparison with the large-scale architectural elements of the Almazán
31 Basin, including fluvial, mudflat, palustrine and lacustrine sedimentary systems. The
32 Paleogene record of the Almazán Basin is particularly suitable to perform this analysis
33 because it integrates most of the continental environments with well-exposed vertical
34 and lateral relationships. The basin shows an outstanding outcrop exposure, which
35 permits three-dimensional reconstructions. To undertake these objectives, the alluvial-
36 lacustrine and fluvial succession (*ca.* 2700 m) in the Gómara monocline has been dated
37 by means of magnetostratigraphy. Magnetic polarity reversals have been mapped
38 along the monocline, and sedimentation rates have been calculated for four key
39 transects in order to assess their lateral changes in relation to different sedimentary
40 environments and basin settings. The new chronostratigraphy of the basin infill can be
41 used to derive a robust time frame for biostratigraphic calibration, and to analyse the
42 tectonosedimentary relationships and the uplift history of the basin.
43
44
45

46 47 **2.- BACKGROUND**

48 49 **2.1. Sedimentary Architecture and Sedimentation Rates**

50
51
52 The architectural changes in both the fluvial systems and their lateral equivalents are
53 often interpreted in terms of changes in the accommodation or in the ratio between
54 accommodation and sediment supply (Muto and Steel, 1997; Carrol and Bohacs, 1999;
55 Bohacs *et al.*, 2000; Huerta *et al.*, 2011). This is a basic assumption of sequence
56 stratigraphy, which contributed to an efficient interpretation of the evolution of
57 depositional systems (Catuneanu *et al.*, 2009). We took the definition of
58
59
60

1
2
3 accommodation provided in Muto and Steel (2000) in which accommodation is seen as
4 “the thickness, measured at a specified site and time, of a space which becomes filled
5 with sediments during a specified time interval”. This definition is practical to quantify
6 because it is equivalent to sedimentation rates. Sediment supply is considered to be
7 the volume of sediment delivered to a certain place of the basin in a given time
8 (sediment deposited + sediment bypassed). This value is difficult to estimate from field
9 data in ancient sedimentary systems. We use the classification of high- and low-
10 sediment supply areas provided in Huerta *et al.*, (2011).
11
12

13 Changes in the large-scale architecture of depositional systems are usually associated
14 to changes in accommodation. Spatial and temporal variability of accommodation
15 leads to a complex interaction throughout sediment distributive systems, affecting the
16 localization of sedimentary environments, the bypass rate, the avulsion frequency and
17 the slope in clastic systems, which also modify the sediment supply. To correctly
18 understand the triggers of changes in large-scale architecture it is therefore needed to
19 identify the accommodation and sediment supply interplay. The ratio between
20 accommodation space and sediment supply (AS/SS) is, however, relative, because field
21 estimations of sediment supply are hardly quantifiable. Relativeness of the AS/SS ratio
22 can be reduced pinning accommodation between intervals sharing sedimentation
23 rates. This allows observing the influence of sediment supply variations in both the
24 large-scale architectural arrangement and the shifts between depositional
25 environments. The LAB models (Leeder-Allen-Bridge; Allen, 1978; Bridge & Leeder,
26 1979) and most studies in ancient sedimentary records show that an increase in
27 accommodation in fluvial settings is related to prevalence of isolated and narrow
28 channels. There are, however, other factors such as the avulsion frequency that should
29 be taken into account. If the avulsion frequency grows faster than sediment
30 accumulation, it can produce high channel interconnection (Heller & Paola, 1996). In
31 addition, some field studies disagree about the inverse relationship between channel
32 density and accommodation space (Tornqvist, 1994; Colombera *et al.*, 2015). Beyond
33 accommodation, we consider the ratio AS/SS, in order to assess the relative influence
34 of sediment supply in the architectural changes.
35
36
37
38
39

40 The external causes affecting the ratio AS/SS in internally drained non-marine basins
41 are climate and tectonics. Climate forcing can be assessed by means of identification of
42 Milankovitch cycles (Hilgen *et al.*, 2014). However, orbital cycles might not be
43 expressed in the sedimentary record if the environment is not sensitive enough or if
44 the tectonic signal is outweighed. Alternatively, another option is to discriminate the
45 slight differences between climate and tectonics in the sedimentary record. Climate,
46 by means of precipitation and evaporation changes, leads to lateral and longitudinal
47 variations of the sediment grain size (Armitage *et al.*, 2011). On the other hand,
48 tectonics can directly affect accommodation space (AS). Models show that an increase
49 of AS results into coarser grain size accumulation in the proximal sites, followed by a
50 reduction in grain size in distal locations (Armitage *et al.*, 2011; Paola & Martin, 2012).
51 However, in non-marine basins, changes in precipitation and or evaporation may
52 modify the accommodation by base level rise or fall. In parallel, tectonics may change
53 SS by promoting uplift and drainage changes in the catchment areas.
54
55
56
57
58
59
60

2.2 Geological Setting

The Almazán Basin in north-central Spain is a thick-skinned piggy-back basin bounded by the Cameros Massif and the Aragonian and Castilian branches of the Iberian Chain (Fig. 1A). It developed on the hanging wall of the Cameros thrust, which moved northwards over the Cenozoic deposits of the Ebro Basin, producing the uplift of the Cameros Massif and the Iberian Chain during the Alpine orogeny (Casas, 1990; Casas-Sainz, 1993; Muñoz-Jiménez & Casas-Sainz, 1997). The Cameros massif is mainly composed by Upper Jurassic-Lower Cretaceous siliciclastics and carbonates, and the Aragonian branch of the Iberian Chain by Mesozoic carbonates and minor evaporites, with a metamorphic Paleozoic basement. Most of the sediment was delivered from these areas, while the Castilian branch of the Iberian Chain only supplied minor amounts of sediment (Huerta, 2007). During the Paleogene, the Almazán Basin was a non-marine isolated basin, which connected towards the west with the Duero Basin during Neogene times through the Aranda-Burgo de Osma corridor (Armenteros & Huerta, 2006).

The Almazán Basin has a flat-bottomed syncline geometry filled by Paleogene and Neogene non-marine deposits, reaching a maximum total thickness of more than 3500 meters at its depocentre (Fig. 1B). The depocentre is bounded by the Almazán and Arcos monoclines towards the south, and the Gómara monocline and the Aragonian branch of the Iberian Chain towards the north (Casas-Sainz *et al.*, 2000). The activity of these structures was synchronous to sedimentation, controlling the distribution and thickness of the stratigraphic units that filled the basin.

2.3. Sequence stratigraphy

Detailed mapping (scale 1:25000), stratigraphic correlations and seismic interpretation in the Almazán Basin were carried out in earlier studies (Huerta, 2007). Further detailed sedimentological, mineralogical and geochemical analyses were performed in the fluvial, lacustrine and playa-lake systems (Huerta *et al.*, 2010; Huerta *et al.*, 2011). On the basis of these studies the complete Paleogene basin infill is divided into four Depositional Sequences (A1 to A4 in Fig. 1). These sequences overlie an unconformity characterised by a hiatus that encompasses from Upper Cretaceous to lower Bartonian, and minor erosion of the Upper Cretaceous marine limestones.

Depositional Sequence A1 crops out close to the northern and eastern basin margins. It reaches a maximum thickness of 400 m, which gradually reduces towards the south and southeast. This sequence denotes a retrogradation from conglomeratic alluvial deposits passing into distal alluvial plains dominated by calcretes and shallow carbonate-precipitating lakes. The Mazaterón mammal fossil site (MP 15-16, Jiménez & Cuesta, 1994) is located at the top of this sequence.

Depositional Sequence A2 crops out principally in the northern domain of the basin, with a maximum thickness of 900 m that wedges out towards the south. The base of the sequence is marked by a change in the sedimentation trend from retrogradational to progradational. A2 expanded southwards on Upper Cretaceous basement rocks, reaching the opposite basin margin.

1
2
3 Depositional Sequence A3 can be observed in the Gómara monocline and in the
4 Torlengua anticline (Fig. 1). It reaches a thickness of 1100 m, wedging out towards the
5 south and southeast, and displaying a progradational trend. The base of the sequence
6 consists of an unconformity, which changes basinwards into a correlative conformity
7 marked by calcretes and gypcretes, indicating a retrogradational trend of the fluvial
8 system. Close to the Aragonian branch, in the Southeast domain (Deza-Embid), its
9 lower boundary consists of an unconformity covering A2 and Upper Cretaceous
10 limestones. Its thickness is notably reduced towards the upper limb of the Gómara
11 monocline (Northern Domain) and on the upper limb of the Almazán monocline at the
12 south of the basin.
13
14

15 Depositional Sequence A4 is covered by undeformed Neogene units, with the
16 exception of few outcrops along the Gómara monocline. In contrast to older Paleogene
17 depositional sequences, it becomes thicker southwards and displays syntectonic
18 unconformities at the basin margins. This sequence is articulated in the Gómara
19 monocline and records the exhumation of the northern domain, evidenced by the
20 occurrence of Paleogene clasts.
21
22

23 **2.4. Tectonic domains**

24

25 The structural framework of the Almazán Basin is divided into five principal tectonic
26 domains (Fig. 1): i) the northern domain; ii) the Almazán and Arcos monoclines; iii) the
27 south-eastern domain; iv) the Gómara monocline; and v) the basin depocentre. A
28 description of the tectonic domains and their structures is provided, except for the
29 basin depocentre, which steadily subsided during all the Paleogene and Neogene
30 history.
31
32

33 The northern domain of the basin (i) records the maximum thickness of A1 and A2. A3
34 is only preserved in the core of two synclines, and A4 is absent (Huerta *et al.*, 2011).
35 This domain is bounded by the Sierra de la Pica Thrust or South Cameros Thrust
36 (Navarro Vázquez, 1991; Guimerà *et al.*, 1995) towards the North, and the Gómara
37 monocline towards the South (Fig. 1). It is affected by NW-SE trending folds plunging
38 towards the NW, which at the same time were affected by perpendicular minor folds.
39 The NW-SE anticlines are bounded by thrusts towards the north, along the Aragonian
40 branch of the Iberian Range.
41
42
43

44 The Almazán and Arcos monoclines (ii) are located in the southern part of the basin,
45 and are only recognizable in subsurface (Casas-Sainz *et al.*, 2002). These monoclines
46 are WNW-ESE oriented, are related to faults affecting the Paleozoic basement, and dip
47 15° to 45° northwards. Folding started during A3 (adapting the Casas-Sainz *et al.*, 2002
48 unit boundaries to our sequence stratigraphic framework), producing a structural relief
49 of about 2000 m in the case of the Almazán monocline (Casas-Sainz *et al.*, 2002).
50 During the initial stages of the monocline development, limb rotation occurred, this
51 evidenced by thickness reduction towards the upper limb. During A3 and A4
52 deposition, the monoclines developed by kink band migration showing excellently
53 preserved growth strata (Casas-Sainz *et al.*, 2002), displaying important thickness
54 reduction in their upper limb.
55
56
57
58
59
60

1
2
3 The south-eastern domain (iii) is characterized by a thickness decrease of the
4 Paleogene succession with respect to the Gómara monocline. The A2/A3 and A3/A4
5 boundaries are marked by unconformities, and important local alluvial fan deposits
6 occur in every depositional sequence boundary in this domain. The La Alameda-Tapiela
7 anticline/thrust (this nomenclature is used for folds that in some parts evolved into
8 thrusts) supplied with sediments the local alluvial fan systems. Southwards, the
9 development of the Torlengua anticline folded the A4 sequence in its northern limb.

10
11
12 The Gómara monocline (iv) was generated in response to the development of the La
13 Alameda-Tapiela anticline/thrust. It connects the northern domain with the basin
14 depocentre. It has NW-SE trend, dips 30° southwards, and generated a structural relief
15 of about 2500 m. Towards the SE, around the Deza area (Fig. 1; Fig. 2), the monocline
16 evolved into a succession of folds. As a consequence, all the Paleogene depositional
17 sequences (A1-A4) were folded, and also a thickness reduction in A3 towards the
18 upper limb of the monocline is observed. A4 has a wedge shape that articulated in this
19 monocline, opening southwards. The outcrops of this structure show a cross-section
20 perpendicular to the main drainage system of the basin.
21
22
23
24

25 **3.-METHODS**

26 **3.1. Channel density calculations**

27
28
29 The channel interconnection or channel density has been quantified mapping the
30 channel fills and the overbank deposits in outcrops of the Gómara monocline. The
31 Channel density is taken as the percentage of the surface in a fluvial succession
32 occupied by channel fills. Eight representative boxes or rectangles of 0.350 km² were
33 drawn in a GIS with its long side parallel to stratification (Fig. 3; Fig. 4). The size of the
34 boxes was in the large-scale size of the fluvial architecture in the sense of Leeder
35 (1993) and Jo & Chough (2001). Four were drawn on the Depositional Sequence A2
36 and four in A3, to have a representation of the channel density of the end-members
37 identified in the fluvial succession. The results are represented in the Table 1 (The
38 mapped boxes are available as supplementary material).
39
40
41

42 **3.2. Magnetostratigraphy**

43
44 Paleomagnetic sampling was performed with an electrical portable drill along the two
45 overlapping Almazul and Mazaterón sections (Fig. 2), encompassing a total thickness of
46 2670 meters. The sampled interval included the alluvial Almazul Fm., the
47 lacustrine/palustrine Mazaterón Fm., and the fluvial Gómara Fm. (Fig.2).
48 Representative sampled lithologies included red and orange mudstones (mainly), very
49 fine sandstones, limestones and marls (occasionally). An optimal sampling transect was
50 chosen to include the most expanded sections with higher abundance of fine grained
51 lithologies, the best outcrop exposures, and stratigraphic continuity. Two cores per site
52 were drilled with an average spacing of 10 meters/site, collecting a total of 269 sites.
53
54

55
56 Samples were analysed in the paleomagnetic laboratories of Fort Hoofdijk (Utrecht
57 University) and the Institute of Earth Sciences Jaume Almera (CCiTUB-ICTJA CSIC). The
58 Natural Remanent Magnetisation (NRM) was measured on DC SQUID superconducting
59
60

1
2
3 rock magnetometers (2G Enterprises Ltd). Stepwise thermal increments were of 50°C
4 up to 350°C, and of 30°C up to the maximum unblocking temperature of samples.
5 Magnetic susceptibility was measured with a KLY-2 susceptibility bridge (Agico) at each
6 demagnetization step in order to monitor mineralogical changes during heating.
7

8 **3.3 Isochrons map and SR calculations**

9
10
11 Magnetostratigraphy provided the location of magnetic reversals for the sampled
12 section. Prominent and laterally continuous beds can be interpreted as isochrones
13 within the magnetostratigraphic temporal resolution. The lateral extension of the
14 reversals was inferred by means of key beds (Fig. 2), which allowed mapping the
15 reversals along the study area. When channels are wide and interconnected or when
16 continuous limestone beds crop out, the mapping results straightforward. However,
17 within mudflats deposits the precision of the correlation decreases. In spite of this, the
18 correlation was possible for the most of the monocline, allowing a fine evaluation of
19 stratigraphic thickness variations across the Paleogene record of the Gómara
20 monocline.
21
22

23
24 Mapping of the magnetic reversals allows the quantification of Sedimentation Rates
25 (SR) for different time intervals (Johnson *et al.*, 1988). Direct measurements were
26 performed along the Miñana section, which is representative of the fluvial system. In
27 this case, the ratio between sediment accumulated and time directly gives SR.
28 Additionally, SR were estimated in 3 other key transects in order to assess the SR
29 variability related to sedimentary environments and basin locations. For these
30 sections, SR were estimated after geometrical calculation of thicknesses between
31 magnetic reversals. Thicknesses were later verified with adjacent stratigraphic logs
32 (Huerta, 2007), and finally plotted against magnetic reversal ages (Table 2). Some
33 restrictions to the SR calculation are that: (i) sedimentation rates are inferred for
34 intervals bounded by polarity reversals, and therefore represent average rates, and (ii)
35 for short intervals the age uncertainty associated to the chron boundaries may lead to
36 significant errors in the inferred SR. This allowed the assessment of SR for all the
37 depositional systems in the monocline. Fluvial system is best represented in the
38 Zárabes transect, mudflats and saline mudflats in the Colmenares transect, and
39 lacustrine-palustrine systems in the Castillejos transect.
40
41
42
43

44 **4.-RESULTS**

45 **4.1. Large-scale architecture**

46
47
48 The Gómara monocline (Fig. 1) accommodates up to 2500 m of sediments comprising
49 Depositional Sequences A1 to A3. The main large-scale architectural elements (LAE)
50 defined are: i) Ribbon-shaped channel fills with low interconnectivity (Fig. 3A); ii)
51 Sheet-like channel fills with high interconnectivity (Fig. 3B); iii) Palustrine/lacustrine
52 Limestone units (Fig 3C and D); iv) Mudstone and evaporitic mudstone units (Fig. 3E);
53 and v) stacked calcretes (Fig. 3F). These LAE pass gradually, vertically and laterally,
54 from one into another. Frequent transitions from ribbon-shaped channel fills with low
55
56
57
58
59
60

1
2
3 interconnectivity to sheet-like channel fills with high interconnectivity occur gradually
4 by means of intermediate stacking patterns.
5

6 i) Ribbon-shaped channel fills with low interconnectivity.
7

8 This LAE is constituted by sandy ribbon-shaped channel fills and red mudstones, with a
9 density of the channel bodies lower than 10% (Table 1; Fig. 4). It is most common in
10 A2, especially in the middle of the sequence, and during A4 (Fig. 2). The channel and
11 channel belt fills never exceed 50 m wide, being their common thickness around 2 m
12 (Fig. 4A). The width/thickness (w/t) ratios typically range from 3:1 to 15:1, although in
13 A4 some channel fills are vertically stacked (multi-storey) forming bodies with 1:3 w/t
14 ratios. These channels are isolated within red mudstones. Middle-scale and simple
15 architectural members are described in Huerta (2007); Huerta *et al.* (2011).
16
17

18 ii) Sheet-like channel fills with high interconnectivity.
19

20 It is constituted by sheet-like conglomerate and sandstone channel fills and red
21 mudstones. Occasionally, calcrete beds are intercalated within the mudstones. The
22 density of the channels is high and ranges from the 20% to 52% (Table 2; Fig. 4). It is
23 most frequent in the upper part of A3, where channels are thicker, and wider (Fig. 4B).
24 The channel and channel belts are wider than 500 m, some exceeding 3000 m.
25 Common thickness is around 5 m, although thicker conglomerate beds (15-35 m) are
26 recorded in the upper part of A3. W/t ratios are higher than 100 and there are no
27 evidences of vertical and lateral accretion. These channels and channel belts are
28 dominated by conglomerates, which in the upper part of A3 contain clasts that can
29 reach up to 70 cm. Laterally to these channel fills calcretes are common. Middle-scale
30 and simple architectural members are described in Huerta (2007); Huerta *et al.* (2011).
31
32
33

34 iii) Palustrine/lacustrine Limestones.
35

36 This unit consist of limestones, dolostones and marls which contain limnic fossils like
37 gastropods, ostracods and charophytes. Reptile and mammal fossils have been
38 occasionally found associated to these units. Carbonate facies have the classical
39 exposition features defined in palustrine deposits, similar to those described by
40 Alonso-Zarza *et al.* (1992); Armenteros *et al.* (1997); Huerta & Armenteros (2005);
41 Alonso-Zarza *et al.* (2006). Calcretes and dolocretes are common in the transitional
42 areas between the limestone and the clastic units (Huerta & Armenteros, 2004). The
43 thickness of the palustrine/lacustrine limestones is about 200 m although it can reach
44 a total thickness of 450 m (Deza Fm.) These units are preferentially found in A1/A2
45 boundary and in A2 (Fig. 2) and occurs in areas close to the basin margin, passing
46 towards distal positions into an evaporitic mudflat. Simple elements and facies of the
47 palustrine/lacustrine units are described in Huerta & Armenteros (2004); Armenteros
48 *et al.* (2006).
49
50
51

52 iv) Mudstones and evaporitic mudstones.
53

54 This unit consist of mudstones and mudstones with interstitial gypsum intercalated
55 with tabular fine-sandstone beds and gypcretes (gypsum crusts). Sandstone channel
56 fills are rare. It crops out in A2 and A3 in the southeastern part of the Gómara
57 monocline and passes laterally into palustrine/lacustrine limestone units and ribbon-
58
59
60

1
2
3 shaped channel fills with low interconnectivity. Simple elements and facies of this LAE
4 are described in Huerta *et al.* (2010) which also describes the playa-lake system
5 containing these deposits.
6

7 v) Stacked calcretes
8

9 This unit is constituted by several metre-scale calcrete profiles stacked vertically. The
10 calcretes ranges from nodular or prismatic at the base to massive at the top. The
11 massive top of a profile is overlapped by the nodular or prismatic horizon of the next
12 profile. In some cases, the superposition of the calcrete profiles blurs the nodular or
13 prismatic structure. In other cases the calcretes are separated by powdery carbonate
14 or by red mudstones. The calcretes are constituted by a microsparitic mosaic with
15 disperse quartz grains and show oxide staining patches and mudstone relics which
16 become smaller towards the upper parts of the profile. This LAE occurs mainly in A3,
17 laterally to the sheet-like channel fills with high interconnectivity. The calcretes and
18 stacked calcretes related to the connection between palustrine/lacustrine units and
19 the clastic units (A1/A2) are similar to those described here but the latter can pass
20 upwards into dolocretes and palustrine/lacustrine limestones (Huerta & Armenteros,
21 2004). The textural and structural features of the stacked calcretes are described in
22 Huerta (2007) and Huerta *et al.* (2011).
23
24
25

26
27 **4.2. Sedimentology**
28

29 Previous sedimentological analysis of simple and medium architectural elements
30 present in the i, ii, and v LAEs, interpret these deposits as parts of a distributive fluvial
31 system with carbonate soils in distal floodplains (Huerta, 2007; Huerta *et al.*, 2011).
32 Ribbon-shaped channels have been interpreted as low sinuosity channels with minor
33 lateral movement some of them showing anastomosis. Sheet-like channels have been
34 interpreted as lateral-stacked channel belts with great mobility across the floodplain
35 and a braided channel pattern. The stacked calcretes are interpreted as distal floodplain
36 areas with important pedogenesis favoured by the low sediment accumulation
37 (Huerta, 2007; Huerta *et al.*, 2011). The LAEs identified in the vertical stacking pattern
38 of fluvial system were laterally related, being the sheet-like channels with high
39 interconnection upstream sections of the ribbon-shaped channels with low
40 interconnection.
41
42

43 The mudstones and evaporitic mudstones have been interpreted as dry mudflats
44 dominated by gypsum precipitation which passed southwards into saline mudflats and
45 constituted a playa-lake system lateral to the main fluvial system (Huerta, 2007;
46 Huerta *et al.*, 2010).
47

48 The dry mudflat passes laterally into limestones and marls with gastropods, ostracods
49 and charophytes. Some beds show exposure features, gypsum pseudomorphs and
50 silica nodules. These carbonates have been interpreted as carbonate precipitating
51 lakes or ponds with low gradient margins which connects with the clastic systems
52 through carbonate soil fringes (calcretes/dolocretes) (Huerta, 2007).
53
54
55
56
57
58
59
60

1
2
3 Alluvial fan sediments fringing the northern margin of the basin are not described here
4 because they are not represented in the Gómara monocline. Only distal alluvial
5 deposits are recorded in A1 (Miñana section).
6

7 **4.3. Magnetostratigraphic results**

8
9
10 Orange to reddish mudstones yielded unblocking temperatures circa 650°C, suggesting
11 that hematite is the principal magnetic carrier. Carbonate rocks yielded unblocking
12 temperatures in general below 600°C, suggesting that magnetite is more dominant in
13 these lithologies. Most of the samples showed a low-temperature component, which is
14 removed after 250°C. The direction of this component in geographic coordinates
15 usually parallels the drilling direction (Fig. 5a, sample MZ236), most likely related to
16 recent viscous acquisition. A high temperature Characteristic Remanent Magnetisation
17 (ChRM) ranging from 350° to the maximum unblocking temperature is found in most
18 of samples and yields both normal and reversed polarity directions. ChRM components
19 were determined after inspection of Zijdeveld plots in 234 samples (86.9 % of total),
20 and directions were calculated by means of principal component analysis (Kirschvink,
21 1980) (Fig. 5a).
22
23

24
25 The stereographic plot of paleomagnetic data in geographic coordinates shows a
26 distribution of normal and reversed polarity directions with low average inclinations
27 (Fig. 5b). Tilt correction for the southwestwards dip of beds yielded steeper mean
28 inclination values, which are more coherent with the Paleogene Iberian plate
29 paleolatitude (Rosenbaum *et al.*, 2002). Antipodality of the mean normal and reversed
30 direction was not achieved, and low inclination values of the reverse samples may be
31 related to partial overlap with a downwards-dipping low temperature secondary
32 component (Fig.5). Westwards deviation of both normal and reverse mean directions
33 could also be related to a partial overlap with drill-induced viscous magnetization. We
34 interpret the low values of the precision parameter (k) as caused by this overlap with
35 secondary components (Fig.5).
36
37

38
39 The paleolatitude of the Virtual Geomagnetic Pole (VGP) was calculated at a sample
40 level and plotted against thickness in order to establish a Local Magnetic Polarity
41 Stratigraphy (LMPS, Fig. 6). Positive paleolatitudes were computed as normal
42 polarities, while negative ones were interpreted as reversed polarities. Normal and
43 reversed magnetozones were defined by at least two adjacent samples of the same
44 polarity. Single-site reversals are depicted as half bar magnetozones in the LMPS plot,
45 and are not considered for magnetostratigraphic correlation purposes. Correlation of
46 the LMPS with the Global Polarity Time Scale (GPTS) was firstly based on
47 biochronological data from the Mazaterón and Deza fossil mammal localities (Badiola
48 *et al.*, 2009), which suggest upper Eocene age. Guided by these constraints, a best
49 correlation of the LMPS to the GPTS 2012 (Gradstein *et al.*, 2012) was obtained by
50 linking the very long reversed magnetozone R8 (Fig. 7) with chron C12R, the
51 characteristic long reversed chron of the early Oligocene. A remarkable positive
52 correlation results for most of the polarity sequence (Fig. 7). Solely the correlation of
53 the normal magnetozone N3 presented some uncertainties. The proposed correlation
54 of N3 with chron C19n yields significantly lower sedimentation rates than average.
55 However, a significant lithology contrast takes place during this interval, with
56
57
58
59
60

1
2
3 occurrence of calcretes indicating pedogenetic processes and environments with low
4 sediment supply. This correlation is also supported by high-resolution
5 magnetostratigraphic studies (Edgar *et al.*, 2010) that find a new normal event within
6 chron C18r which would correlate with the short normal magnetozone within R3 in the
7 Mazaterón Formation (Fig. 7).
8

9 10 **4.4. Age of Depositional Sequences and biostratigraphic** 11 **calibration**

12 The most remarkable pattern shown by the isochrons map (Fig. 8) was the thicknesses
13 variations, showing a wedging towards the East. This wedging is associated with an
14 eastern gradual reduction of clastic sedimentation. In addition, the map reveals that
15 variable widths between isochrones can be significant between adjacent areas, and
16 that this relationship may change throughout time. The map also provides information
17 for dating the depositional sequences boundaries across the basin, and the fossil sites
18 located within the sequences.
19
20

21 The magnetostratigraphic study presented here provides a robust temporal framework
22 for the Depositional Sequences of the Almazán Basin (Fig. 7). Depositional Sequence
23 A1 is found to encompass from chron C21n to C18r, lasting *ca.* 5 Myr (Fig. 7).
24 Depositional Sequence A2 encompasses from chron C18r to chron C13r, with duration
25 of 5.8 Myr, and including most of the Bartonian and Priabonian Stages. Depositional
26 Sequence A3 lasts 6.6 Myr, from chron C13r to chron C9n, comprising the end of
27 Priabonian, Rupelian and part of the Chattian. The Eocene/Oligocene boundary is
28 placed near the base of A3 (Fig. 7). Magnetostratigraphic data are not available for
29 Depositional Sequence A4 because this unit remains buried in the Gómara monocline,
30 and ages can only be interpolated by means of seismic profiles.
31
32
33

34 The Mazaterón mammal fossil locality (MP 15-16, Cuesta & Jiménez, 1994), in the
35 lower part of the Mazaterón Formation (Fig. 7), correlates to chron C18r (Lower
36 Bartonian), in agreement with previous biochronological interpretations (Cuesta &
37 Jiménez, 1994). The isochrons map allows dating the mammal fossil locality of Deza 2
38 (MP 17b, Badiola *et al.*, 2009), yielding a correlation with Chron C15r, at mid-
39 Priabonian (Fig. 8).
40
41

42 **4.5. Sedimentation Rates**

43 In order to assess the variability of SR both in time and space, the combined isochron
44 map and bedding orientation data were used for calculation of SR along the different
45 sections within the Gómara monocline. The results are shown in Fig. 9, where SR data
46 is provided for every time-slice given by magnetostratigraphic reversals.
47
48
49

50 The general trend of SR shows pronounced shifts which are coincident with sequence
51 boundaries. Both the A1/A2 and the A2/A3 boundaries are marked by increases of SR.
52 Lateral changes in SR are associated to gradual changes of the depositional systems,
53 which can be tentatively ordered from higher to lower SR. Although some exceptions
54 exist, higher SR occur in fluvial systems, and gradually decrease in mudflat to lacustrine
55 and finally palustrine settings with aerial exposition features. The principal exceptions
56
57
58
59
60

1
2
3 occur in the mudflats or lacustrine systems which may present higher rates than
4 certain fluvial intervals.
5

6 Within the fluvial system, highest SR are related to more isolated ribbon-like channels,
7 while lowest SR are related to intervals of more amalgamated and wider channels.
8 Ribbon-like channels develop when rates are above 25 cm/kyr, and amalgamated
9 sheets occur when rates are below 12 cm/kyr. Between these values mixed
10 architectures develop. Adjacent to the fluvial system, the mudflats yield SR which
11 increase with the mud proportion and typically fluctuate between 14 to 23 cm/kyr.
12 Finally, lacustrine systems lacking features indicating aerial exposure yield SR close to 9
13 cm/kyr, whereas the intervals dominated by calcrete accumulation record 3 cm/kyr.
14 This indicates that net calcrete accumulation is below 3 cm/kyr because the averaged
15 intervals include other deposits apart from calcretes.
16
17
18

19 20 21 **5.-DISCUSSION**

22 **5.1. Basin fill and tectonic history**

23 **Depositional sequence A1**

24
25
26 Deposition in A1 begins as accommodation is created due to the Cameros thrust
27 emplacement. The sedimentation grades upwards from distal alluvial to a calcrete
28 fringe and palustrine-lacustrine environments. The average SR in the Miñana section
29 (Figs. 8 and 9) show a change from 4.7 to 6.3 cm/kyr in the alluvial deposits. A
30 decrease to 3 cm/kyr is related to the occurrence of stacked calcretes and
31 palustrine/lacustrine limestones representing the carbonate soil fringe in the
32 connection between the distal alluvial and the carbonate precipitating lake/pond. The
33 increase in the SR recorded in the carbonates from Miñana section (13.5 cm/kyr) is
34 related to an increase in the palustrine/lacustrine facies at the upper part of A1. This is
35 interpreted as the beginning of a period with increasing AS which consolidates during
36 A2.
37
38
39

40 Laterally, towards the Zárabes section (Fig. 8), the palustrine and lacustrine facies pass
41 into fluvial deposits with wide and lateral amalgamated channels. SR of the fluvial
42 deposits show an average of 7.4 cm/kyr. Similar SR values in the Zárabes and Miñana
43 sections suggest that AS in the fluvial system is similar to the laterally related
44 palustrine/lacustrine environments, but the sedimentary supply in the fluvial system
45 hinders the expansion of the lake.
46
47

48 The beginning in AS creation around A1/A2 boundary and the increase in SS recorded
49 by the development of the Gómara fluvial system is likely linked to an increase of the
50 uplift in the Cameros Massif, which underwent maximum uplift rates at around 40 Ma
51 as indicated by fission track data (Del Rio *et al.*, 2009). The uplift was transferred to the
52 Almazán Basin by the activity of the Cameros thrust and, principally, by the inception
53 of the South Cameros Thrust (SCT), and La Alameda Thrust (ATT; Fig. 10; Fig. 1 for
54 location).
55
56

57 **Depositional sequence A2**

1
2
3 The sedimentation in A2 shows a broadening of the deposition areas towards the
4 South and East (Fig. 10). The development of SCT and ATT provided additional
5 accommodation space and an increase of sediment supply. The fluvial systems
6 (Zárabes area) reflect an increase of SR to 15.5 cm/kyr, whereas the lacustrine
7 environments of the Miñana section gradually shifted to fluvial deposits with rates
8 slightly lower than in Zárabes (Fig. 9). In mid A2, the area experiencing more
9 accommodation was Miñana instead of Zárabes. This is reflected in both
10 sedimentation rates and in the Large-scale architectural pattern. The Miñana section
11 show a sharp SR increase up to 40.1 cm/kyr and ribbon-shaped channels with low
12 interconnection. Contrastingly, the Zárabes section yields SR of 8.1 cm/kyr, at this
13 interval characterized by a higher channel density and width.
14
15

16
17 Towards the SE the fluvial deposits pass into a dry mudflat formed by mudstones and
18 evaporitic mudstones (Colmenares section). In the mudflat SR were slightly lower than
19 in the fluvial system, suggesting that the change in the architectural pattern, with the
20 absence of channel fills, is driven by a lateral reduction in clastic supply. Further east,
21 palustrine/lacustrine limestone units (Deza deposits) reveal a extreme reduction in
22 sediment supply allowing the development of lakes and ponds (Huerta *et al.*, 2011)
23 that are filled by bio-chemical precipitation (SR of 9 cm/kyr, Castillejos section). The
24 overall decrease of the sediment supply towards the East occurred during A2, in
25 synchrony with fold growth in the Aragonian branch. Relief generation in this basinal
26 domain controlled the main fluvial transfer system, and sheltered the eastern sectors
27 from receiving significant clastic contributions. Towards the top of A2, a general
28 reduction in accommodation is deduced from the decreasing SR in all the sections
29 (Fig.9). This trend caused channel amalgamation in fluvial units and calcrete
30 occurrence in their lateral mudflat deposits.
31
32
33

34 **Depositional sequence A3**

35
36 The A2/A3 boundary correlates with the activity of existing and newly formed tectonic
37 structures (Fig. 10), giving rise to unconformities at the basin margins. During A3 the
38 Gómara monocline was active, generating large AS in the lower limb and reducing AS
39 in the upper limb. SR strongly responded to these changes, increasing to 45.6 cm/kyr
40 in the Zárabes section, and 27.5 cm/kyr in the Miñana section. This stage is marked by
41 ribbon-shaped channel fills with low interconnection in the Zárabes section that
42 laterally became wider and more amalgamated towards the Miñana section. Their
43 lateral equivalent mudflat sediments yield lower SR values (15.5 cm/kyr). The
44 southeastwards decrease in SR is interpreted as driven by accommodation changes
45 related to the position relative to the monocline limbs, the Zárabes section closer to
46 the lower limb, and the Miñana and Colmenares sections closer to the upper limb.
47 Neither the sediment supply pattern nor the distribution of the paleocurrents shows
48 any significant change during this period.
49
50
51

52 A meter-thick fossil-rich calcrete yields interbedded within the A3 fluvial sequence in
53 the Miñana section (near the Mazaterón village, Fig 2). The occurrence of this layer
54 could record a decrease in sediment supply following the ideas of Carrol & Bohacs
55 (1999); Bohacs *et al.* (2000); Huerta *et al.* (2011). Since magnetostratigraphic
56 correlation brings this bed at near the Eocene-Oligocene boundary, it is plausible that
57 it represents a transient climatically-forced reduction of the sediment input. We note,
58
59
60

1
2
3 however, that long-term architectural trends remain, with no sights of irreversible
4 changes related to the transition into the icehouse world.
5

6 Towards the upper part of A3, a significant reduction in SR is observed in all the
7 sections (Fig.10). SR gradually decrease in the Zárabes section from values around 20
8 cm/kyr to below 10 cm/kyr (Fig. 9). Same trend, but delayed with respect to Zárabes, is
9 observed in the Miñana section, decreasing from 20 to 10 cm/kyr. The reduction in SR
10 is associated to the occurrence of the sheet-like channel fills with high interconnection.
11 This is interpreted as a reduction in AS produced by the uplift of the Gómara
12 monocline in its upper limb. The reduction in AS favours the lateral expansion of the
13 fluvial system which is recorded in the Colmenares section and the migration of the
14 fluvial depocentre southwards towards the basin centre (See Fig.1B).
15
16

17 **Depositional sequence A4**

18
19 Previous studies (Huerta 2007; Huerta *et al.*, 2011) showed that A4 (Chattian to
20 Miocene) records the uplift and erosion of the northern domain of the basin, and
21 coarse alluvial fan deposits with internal unconformities occur at the southeast domain
22 (Deza-Embida area). A4 articulates in the Gómara monocline displaying syntectonic
23 unconformities and becoming thicker southwards. This stratal pattern, the occurrence
24 of ribbon-shaped channel fills with low interconnection, and the unroofing of the
25 northern domain suggest that although sedimentation rates have not been calculated
26 for this depositional sequence, both AS and SS were relatively high.
27
28

29 **5.2. Accommodation, Sediment supply, and Large-scale** 30 **architecture.** 31 32

33
34 Sedimentation rates reflect the accommodation space for a specific site and time
35 interval, following Muto and Steel (2000). The SR calculated in the Gómara monocline
36 (Almazán Basin) help us assessing the relationship between the large-scale
37 sedimentary architecture and the accommodation space and sediment supply.
38

39
40 As seen above, sheet-like channel fills with high interconnectivity LAE occur at times of
41 lower accommodation space (see upper part of the A3 with SR around or below 10
42 cm/kyr) than the ribbon-shaped channel fills with low interconnectivity (see A2 with SR
43 around 30-40 cm/kyr) (Fig. 9). In this scenario, low SR reflect the low aggradation of
44 the floodplains favouring lateral mobility and an increase of channel density, while
45 high SR reflect an important aggradation of the floodplain which favoured avulsion and
46 predominance of isolated channels (Bryant, 1995). This is consistent with data from
47 experimental models which indicate that the higher SR are recorded in floodplains
48 while channels only act as conduits for sediment bypass (Sheets *et al.*, 2002). It is
49 important to note that the two LAE discussed above develop in high sediment supply
50 conditions as revealed by the clast size and the sedimentary system arrangement.
51
52

53
54 The distal and lateral reductions in SS are evidenced by the grain-size fining trend
55 from the fluvial system to the mudflats and lacustrine environments. The AS in the
56 palustrine/lacustrine limestone units (SR around 9 cm/ky) is lower than in the
57 correlative mudflats mudstones (SR around 15-20 cm/kyr), and these lower than in the
58
59
60

1
2
3 correlative ribbon-shaped channel fills with low interconnection. This lateral/distal
4 reduction of AS is associated to a reduction in the SS.

5
6 Stacked calcretes reflect the lowest AS (SR around 3 cm/kyr) and low sediment supply
7 as deduced from their location in the distal floodplain, distal alluvial and dry mudflats
8 equivalent to sheet-like channels with high interconnections. This is in agreement with
9 the occurrence of calcretes in low deposition settings (Tandon *et al.*, 1998), sheltered
10 (Armenteros & Huerta, 2006) or uplifting regions (Alonso-Zarza *et al.*, 1999).

11
12 The study of ancient fluvial systems shows marked differences in sedimentation rates,
13 these ranging over two orders of magnitude. When fluvial systems are analysed in the
14 long term (SRS 9-10 of Miall, 2014), most of the data fall within the range given in the
15 compilation work of Colombero *et al.*, (2015), with sedimentation rates between 55-60
16 cm/kyr and 1 cm/kyr. For example, SR for the Siwalik sections in Pakistan average 12
17 cm/kyr (Johnson *et al.*, 1988) and the fluvial deposits of the Junggar Basin (China)
18 around 24.5 cm/kyr (Ji *et al.*, 2008). The overbank and paleosol alternation of the
19 Bighorn Basin (Wyoming) show that average rates are in the range between 40 cm/kyr
20 and 28.8 cm/kyr (Abels *et al.*, 2013). Similarly, sedimentation in mudflat deposits yields
21 values that easily overcome one order of magnitude. Abels *et al.*, (2011), in the Tibetan
22 Plateau, show SR of about 4.6 cm/kyr in mudflat environments, down to 2.1 cm/kyr in
23 gypsiferous mudflats. In the Calatayud-Daroca basin (central Spain) mudflat-dominated
24 deposits record SR rates of about 5 cm/kyr (Abdul-Aziz *et al.*, 2000). In lacustrine
25 settings SR vary over a narrower range, from 10 cm/kyr in the Green River Basin (Smith
26 *et al.*, 2008), to 6-10 cm/kyr in the Oligocene fresh water lacustrine deposits of the
27 Ebro Basin (Valero *et al.*, 2014), and 6.5 cm/kyr in the Junggar Basin (Ji *et al.*, 2008).
28 Variations in lacustrine settings depend on the local subsidence, source area,
29 paleoproductivity and the over- or underfilling state of the basin (Carroll & Bohacs,
30 1999). Finally, the calcretes are suggested to form when pedogenesis overcome
31 sedimentation rates (Machette, 1985) and Daniels *et al.*, (2003) stated that 0.5 cm/kyr
32 is the threshold rate of pedogenic assimilation. The rate of local subsidence and the
33 type of calcretes may increase this range as fine interbedding with other deposits is
34 common. SR for calcretes are thought to be in a range between less than 3 cm/kyr and
35 punctual negative sedimentation.

36
37 The balance between AS and SS represents the response of the basin to external
38 forcing. Size, slope, tectonic evolution and the nature of the source areas are specific
39 of each basin. Thus it may be inaccurate to extrapolate absolute rates to other basins.
40 However, the relative vertical and lateral variations and their relationship to the
41 balance between accommodation and sediment supply may be shared with other
42 sedimentary records.

43 44 45 46 47 48 49 50 **5.3 Climate and tectonics**

51
52 Lateral changes in accommodation space and sediment supply in the Almazán Basin
53 are mainly driven by the tectonic uplift of the Cameros Massif and the Iberian Chain.
54 This is supported by the sequence stratigraphy of the basin, and the documented
55 relationship between sedimentary unconformities and tectonic structures.
56 Palaeocurrents, clast composition and clay mineralogy analyses were carried in order
57 to identify the role of tectonics during basin filling (Huerta, 2007). Thrusting and
58
59
60

1
2
3 folding along the margins provided the basin with sediments and the regional flexural
4 subsidence that supports long-term accommodation. On the other hand, intrabasinal
5 thrusting modified the sediment routing system and contributed to the localized
6 generation or destruction of accommodation space.
7

8
9 Despite the buffering of the upstream signal in large to medium drainage systems
10 (Castelltort & Van Der Driessche, 2003), it has been shown that fluvial deposits can
11 record climatic oscillations (Abels *et al.*, 2013). Recent studies in the Teruel Basin
12 suggest that the superimposition of climate and tectonics exerts an important control
13 on lacustrine sedimentation and in the expansion and retraction of the lake deposits
14 (Alonso-Zarza *et al.*, 2012; Ezquerro *et al.*, 2014). In other basins of the Iberian Chain,
15 the main sedimentary ruptures are not found to correlate with climate change (López
16 Martínez *et al.*, 1987; Calvo *et al.*, 1993; Muñoz-Jiménez & Casas-Sainz, 1997). Added
17 to this complexity, it has been shown that the autogenic response of the sedimentary
18 systems can produce organized stratal patterns with no need of external control (Hajek
19 *et al.*, 2012).
20
21

22
23 In the Almazán basin, well defined large-scale architectural trends occur at basin scale,
24 thus indicating external forcing. No evidence of climate forcing, such as recognition of
25 orbital cyclicity or correlation with global events, is found at this scale. The singularity
26 of a calccrete bed at near the Eocene-Oligocene boundary could represent a
27 climatically-driven transient decrease in the sediment input, but no remarkable shift in
28 the overall sedimentary stacking pattern can be associated to this global scale climate
29 transition. Thus, the occurrence of long-term orbital cycles in the Paleogene fluvial
30 record of the Almazán basin remains not demonstrated. Further research focussed on
31 the evaporitic mudflats and lacustrine/palustrine limestones could provide useful
32 information on this issue.
33
34

35 6.-CONCLUSIONS

36
37
38 The magnetostratigraphy for the Paleogene continental record of the Almazán Basin
39 allows filling a gap of the Cenozoic chronostratigraphy of the Spanish basins. This work
40 permits settling ages of the fossil mammal sites and the depositional sequence
41 boundaries of the basin. In addition, the new ages provide the resolution needed to
42 quantify of sedimentary rates throughout the Gómara Monocline. The combined
43 evolution of depositional sequences, the architectural shifts, and the variations of
44 sedimentation rates are interpreted in terms of accommodation and sediment supply
45 changes.
46
47

48
49 The magnetostratigraphic results reveal that the first depositional sequence A1 started
50 in mid-Lutetian times (chron C21n) in relation to the emplacement of the Cameros
51 Main thrust. The development of the South Cameros Thrust started in early Bartonian
52 (chron C18r), synchronously to deposition of A2. Close to the Eocene/Oligocene
53 transition sedimentation of A3 starts, coeval to the growth of the Gómara, Almazán
54 and the Arcos monoclines, and associated structures, producing differential changes in
55 accommodation space. Since middle Chattian (chron C9n.1n), A4 records the increase
56 in the tectonic activity. The uplift of the Gómara monocline produced the erosion of
57
58
59
60

1
2
3 the northern domain and created growth strata that articulated in the Gómar
4 monocline.

5
6 Relative changes in SR show a correspondence with the large-scale sedimentary
7 architecture, and relative changes in the AS/SS ratio reveal useful for stratal pattern
8 prediction. In areas with high sediment supply, higher SR (30-40 cm/kyr) are related to
9 ribbon-shaped isolated channel fills (channel density < 10%) and predominance of
10 floodplain fine grained deposits. On the other hand, lower SR (< 10 cm/kyr) correspond
11 to laterally extensive sheet-like interconnected channel fills (channel density from 20
12 to 50%) and an increase in the average grain size.

13
14
15 In basin sectors with low sediment input, the predominance of fine sediments,
16 mudstones and evaporitic mudstones reveals a slight decrease in sedimentation rates
17 (SR around 15-20 cm/kyr) with respect to the areas with high sediment supply (fluvial
18 system). Palustrine/lacustrine limestone units occur in areas of very low sediment
19 input and low sedimentation rates (SR around 9 cm/ky) which are reflecting the
20 carbonate production. Stacked calcrete profiles develop in areas with low sediment
21 supply and very low sedimentation rates (SR around 3 cm/kyr) related to distal alluvial
22 or distal floodplain areas.
23
24
25
26
27

28 **Acknowledgments**

29
30 This research was funded by the Spanish projects COFORSED (CGL2010-17479) and
31 SEROS (CGL2014-55900-P), and the Research Group of “Geodinàmica i Anàlisi de
32 Conques” (2014SGR467). LV acknowledges the University of Barcelona for financial
33 support (APIF-UB). Thanks to Cor Langereis, Tom Mullender and Maxim Krasnoperov
34 from the Fort Hoofdijk Paleomagnetic Laboratory (Utrecht University), and to the
35 Barcelona Paleomagnetic Laboratory (CCiTUB-ICTJA CSIC). We are very grateful to the
36 Editor Sébastien Castelltort, and to Liz Hajek, Ana Alonso-Zarza and an anonymous
37 reviewer for their valuable comments on the manuscript. This is a contribution to the
38 ESF Research Networking Programme EARTHTIME-EU (08-RNP-017) and the
39 Geomodels Institute (Universitat de Barcelona).
40
41
42

43 **References**

- 44
45 ABDUL-AZIZ, H., HILGEN, F., KRIJGSMAN, W., SANZ & E., CALVO, J.P., (2000) Astronomical
46 forcing of sedimentary cycles in the middle to late Miocene continental Calatayud
47 Basin (NE Spain). *Earth Planet. Sci. Lett.*, **177**, 9-22
48 ABELS, H. A., KRAUS, M. J., GINGERICH, P. D. (2013) Precession-scale cyclicity in the fluvial
49 lower Eocene Willwood Formation of the Bighorn Basin, Wyoming (USA).
50 *Sedimentology*, **60**, 1467–1483. doi: 10.1111/sed.12039
51 ABELS, H. A., DUPONT-NIVET, G., XIAO, G. Q., BOSBOOM, R., & KRIJGSMAN, W. (2011) Step-
52 wise change of Asian interior climate preceding the Eocene-Oligocene Transition
53 (EOT). *Paleogeogr. Paleoclimatol., Palaeocol.*, **299**, 399-412
54 ALLEN, J.R.L. (1978) Studies in fluvial sedimentation: An exploratory quantitative model for
55 the architecture of avulsion-controlled alluvial suites: *Sediment. Geol.*, **21**, p. 129– 147,
56 doi:10.1016/0037-0738(78)90002-7.
57
58
59
60

- 1
2
3 ALONSO-ZARZA, A.M., CALVO, J.P. & GARCÍA DEL CURA, M.A. (1992). Palustrine sedimentation
4 and associated features -grainification and pseudo-microkarst- in the Middle Miocene
5 (Intermediate Unit) of the Madrid Basin, Spain. *Sediment Geol*, **76**, 43-61.
- 6 ALONSO-ZARZA, A.M., SOPEÑA, A. AND SANCHEZ-MOYA, Y., (1999). Contrasting palaeosol
7 development in two different tectonic settings: the Upper Buntsandstein of the
8 Western Iberian Ranges, Central Spain. *Terra Nova*, **11**, 23-29.
- 9 ALONSO-ZARZA, A.M., (2003). Palaeoenvironmental significance of palustrine carbonates and
10 calcretes in the geological record. *Earth-Sci. Rev.*, **60**, 261-298.
- 11 ALONSO-ZARZA, A.M., DORADO-VALIÑO, M., VALDEOLMILLOS-RODRÍGUEZ, A. & RUIZ-ZAPATA,
12 M.B. (2006). A recent analogue for palustrine carbonate environments: The
13 Quaternary deposits of Las Tablas de Daimiel wetlands, Ciudad Real, Spain. In:
14 *Paleoenvironmental record and applications of calcretes and palustrine carbonates* (Ed.
15 by A.M. Alonso-Zarza & L.H. Tanner), *Geol. Soc. London, Spec. Publ*, **416**, pp. 153-168.
- 16 ALONSO-ZARZA, A., MELÉNDEZ, A., MARTÍN-GARCÍA, R., HERRERO, M.J., & MARTÍN-PÉREZ, A.,
17 (2012) Discriminating between tectonism and climate signatures in palustrine
18 deposits: Lessons from the Miocene of the Teruel Graben, NE Spain. *Earth-Sci. Rev.*,
19 **113**, 141-160
- 20
21 ARMENTEROS, I., DALEY, B. & GARCIA, E. (1997). Lacustrine and palustrine facies in the
22 Bembridge Limestone (late Eocene, Hampshire Basin) of the Isle of Wight, southern
23 England. *Palaeogeogr Palaeoclimatol Palaeoecol*, **128**, 111-132.
- 24 ARMENTEROS, I., BUSTILLO, M.A. & HUERTA, P. (2006). Ciclos climáticos en un sistema lacustre
25 marginal perenne carbonatado-evaporítico. Formación Deza, Eoceno superior, cuenca
26 de Almazán. *Geo-temas*, **9**, 25-30.
- 27 ARMENTEROS, I. & HUERTA, P., (2006). The role of clastic sediment influx in the formation of
28 calcrete and palustrine facies: A response to paleographic and climatic conditions in
29 the southeastern Tertiary Duero basin (northern Spain). *Geol. Soc. Am. S.* **416**, 119–
30 132. doi:10.1130/2006.2416(08).
- 31 ARMITAGE, J.J., DULLER, R.A., WHITTAKER, A.C. & ALLEN, P. (2011) Transformation of tectonic
32 and climatic signals from source to sedimentary archive. *Nat. Geosci.*, **1**–5,
33 DOI:10.1038/NCEO1087
- 34 BADIOLA, A., CHECA, L., CUESTA, M.A., QUER, R., HOOKER, J.J., ASTIBIA, H., NATURAL, T. &
35 MUSEUM, H., (2009). The role of new Iberian finds in understanding European Eocene
36 mammalian paleobiogeography. *Geol. Acta* **7**, 243–258. doi:10.1344/105.000000281.
- 37 BOHACS, K.M., CARROLL, A.R., NEDE, J.E. & MANKIROWICZ, P.J. (2000) Lake-Basin Type, Source
38 Potential and Hydrocarbon Character: An Integrated Sequence-Stratigraphic-
39 Geochemical Framework. In: *Lake Basins through Space and Time* (Ed. by E. H.
40 Gierlowski-Kordesch & K. R. Kelts), *Aapg Studies in Geology*, **46**, 3-33. American
41 Association of Petroleum Geologists, Tulsa, Ok., U.S.A.
- 42 BRIDGE, J.S. & LEEDER, M.R. (1979). A simulation model of alluvial stratigraphy.
43 *Sedimentology*, **26**, 617-644.
- 44 BRYANT, M., FALK, P. & PAOLA, C. (1995). Experimental study of avulsion frequency and rate of
45 deposition. *Geology*, **23**, 365-368.
- 46 CALVO, J.P., DAAMS, R., MORALES, J., LÓPEZ MARTÍNEZ, N., AGUSTÍ, J., ANADÓN, P., ARMENTEROS, I.,
47 CABRERA, L., CIVIS, J., CORROCHANO, A., DÍAZ MOLINA, M., ELIZAGA, E., HOYOS, M., MARTÍN-
48 SUÁREZ, E., MARTÍNEZ, J., MOISSENET, E., MUÑOZ, A. & PÉREZ GARCÍA, A. (1993) Up-to-Date
49 Spanish Continental Neogene Synthesis and Paleoclimatic Interpretation. *Revista de la*
50 *Sociedad Geológica de España*, **6**, 29-40.
- 51 CARROLL, A.R. & BOHACS, K.M. (1999) Stratigraphic Classification of Ancient Lakes: Balancing
52 Tectonic and Climatic Controls. *Geology*, **27**, 99-102.
- 53 CASAS-SAINZ, A.M. (1993). Oblique tectonic inversion and basement thrusting in the Cameros
54 Massif (Northern Spain). *Geodin. Acta*, **6**, 202-216.
- 55
56
57
58
59
60

- 1
2
3 CASAS-SAINZ, A.M., CORTÉS-GARCÍA, A.L. & MAESTRO-GONZÁLEZ, A., (2000). Intraplate
4 deformation and basin formation during the Tertiary within the northern Iberian plate:
5 origin and evolution of the Almazán basin. *Tectonics*, **19**, 258-289.
- 6 CASAS-SAINZ, A.M., CORTÉS, A.L. & MAESTRO, A. (2002). Sequential limb rotation and kink-
7 band migration recorded by growth strata, Almazán Basin, North Spain. *Sediment Geol*,
8 **146**, 25-45.
- 9 CASAS, A.M. (1990). El frente Norte de la Sierra de Cameros: Estructuras cabalgantes y campo
10 de esfuerzos. PhD Thesis, Universidad de Zaragoza, Zaragoza.
- 11 CASTELLTORT, S. & VAN DER DRIESSCHE, J. (2003) How plausible are high-frequency sediment
12 supply-driven cycles in the stratigraphic record? *Sediment. Geol.*, **157**, 3-13
- 13 CATUNEANU, O. & ELANGO, H.N. (2001). Tectonic control on fluvial styles: The Balfour
14 formation of the Karoo Basin, South Africa. *Sediment Geol*, **140**, 291-313.
- 15 CATUNEANU, O. (2006). *Principles of Sequence Stratigraphy*. Elsevier, Amsterdam.
- 16 CATUNEANU, O., ABREU, V., BHATTACHARYA, J.P., BLUM, M.D., DALRYMPLE, R.W.,
17 ERIKSSON, G., FIELDING, C.R., FISHER, W.L., GALLOWAY, W.E., GIBLING, M.R., GILES,
18 K.A., HOLBROOK, J.M., JORDAN, R., KENDALL, C.G. ST.C., MACURDA, B., MARTINSEN,
19 O.J., MIAL, A.D., NEAL, J.E., NUMMEDAL, D., POMAR, L., POSAMENTIER, H.W., PRATT,
20 B.R., SARG, J.F., SHANLEY, K.W., STEEL, R.J., STRASSER, A., TUCKER, M.E. & WINKER, C.
21 (2009) Towards the standardization of sequence stratigraphy. *Earth-Science Reviews*,
22 **92**, 1–33
- 23
24 COLOMBERA, L., MOUNTNEY, N. P., & MCCAFFREY, W. D. (2015). A meta-study of relationships
25 between fluvial channel-body stacking pattern and aggradation rate: Implications for
26 sequence stratigraphy. *Geology*, **43**(4), 283-286
- 27 CUESTA, M.A. & JIMÉNEZ, E., (1994). Síntesis del Paleógeno del borde oriental de la cuenca de
28 Almazán (Soria): Vertebrados de Mazaterón. *Stud. Geol. Salmatic*. XXIX, 157–170.
- 29 DANIELS, J. M. (2003) Floodplain aggradation and pedogenesis in a semiarid environment.
30 *Geomorphology*, **56**, 225-242
- 31 DEL RIO, P., BARBERO, L., & STUART, F.M., (2009). Exhumation of the Sierra de Cameros
32 (Iberian Range, Spain): constraints from low-temperature thermochronology. *Geol.*
33 *Soc. London, Spec. Publ.* 324, 153–166. doi:10.1144/SP324.12
- 34 EDGAR, K.M., WILSON, P. A., SEXTON, P.F., GIBBS, S.J., ROBERTS, A. P. & NORRIS, R.D., (2010).
35 New biostratigraphic, magnetostratigraphic and isotopic insights into the Middle
36 Eocene Climatic Optimum in low latitudes. *Palaeogeogr. Palaeoclimatol. Palaeoecol.*
37 **297**, 670–682. doi:10.1016/j.palaeo.2010.09.016.
- 38 EZQUERRO, L., LUZÓN, A., NAVARRO, M., LIESA, C.L. & SIMÓN, J.L. (2014) Climatic Vs. Tectonic Signals
39 in a Continental Extensional Basin (Teruel, Ne Spain) from Stable Isotope ($\delta^{18}\text{O}$) and
40 Sequence Stratigraphical Evolution. *Terra Nova*, **26**, 337-346.
- 41 FOIX, N., PAREDES, J.M. & GIACOSA, R.E. (2013). Fluvial architecture variations linked to
42 changes in accommodation space: Río Chico Formation (Late Paleocene), Golfo San
43 Jorge basin, Argentina. *Sediment Geol.*, **294**, 342-355.
- 44 GUIMERÀ, J., ALONSO, A., & MAS, R. (1995). Inversion of an Extensional Ramp Basin by a
45 Neofomed thrust: The Cameros Basin (N Spain). In: *Basin Inversion* (Ed. by J.G.
46 Buchanan & P.G. Buchanan), *Geological Society Special Publication*, **88**, 433-453.
- 47 GRADSTEIN, F.M., OGG, J.G., SCHMITZ, M. & OGG, G., (2012). The Geologic Time Scale 2012.
48 Elsevier, Cambridge University Press, Cambridge.
- 49 HAJEK, E.A., HELLER, P.L. & SCHUR, E.L. (2012) Field Test of Autogenic Control on Alluvial
50 Stratigraphy (Ferris Formation, Upper Cretaceous-Paleogene, Wyoming). *Geological*
51 *Society of America Bulletin*, **124**, 1898-1912.
- 52 HELLER, P.L. & PAOLA, C. (1996). Downstream changes in alluvial architecture: an exploration
53 of controls on channel-stacking patterns. *J. Sediment. Res.*, **66**, 297-306.
- 54
55
56
57
58
59
60

- 1
2
3 HELLER, P.L., PAOLA, C., HWANG, I.-G., JOHN, B. & STEEL, R.J. (2001). Geomorphology and
4 sequence stratigraphy due to slow and rapid base-level changes in an experimental
5 subsiding basin (XES 96-1). *Am. Assoc. Petr. Geol. B.*, **85**, 815-838.
- 6 HICKSON, T.A., SHEETS, B.A., PAOLA, C. & KELBERER, M. (2005). Experimental test of tectonic
7 controls on three-dimensional alluvial facies architecture. *J. Sediment. Res.*, **75**, 710-
8 722.
- 9 HILGEN, F.J., HINNOV, L.A., ABDUL AZIZ, H., ABELS, H.A., BATENBURG, S., BOSMANS, J.H.C., DE
10 BOER, B., HÜSING, S.K., KUIPER, K.F., LOURENS, L.J., RIVERA, T., TUENTER, E., VAN DE
11 WAL, R.S.W., WOTZLAW, J.-F., ZEEDEN, C. (2014). Stratigraphic continuity and
12 fragmentary sedimentation: the success of cyclostratigraphy as part of integrated
13 stratigraphy. In: *Strata and Time: Probing the Gaps in Our Understanding* (Ed. by D. G.
14 Smith, R. J., Bailey, P. M, Burgess, & A. J., Fraser) Geol. Soc. London Spec. Publ., **404**.
15 doi: 10.1144/SP404.12
- 16 HUERTA, P. & ARMENTEROS, I. (2004). Asociaciones de carbonatos continentales en el Eoceno
17 de la Cuenca de Almazán. *Geo-temas*, **6**, 75-78.
- 18 HUERTA, P. & ARMENTEROS, I. (2005). Calcrete and palustrine assemblages on a distal alluvial-
19 floodplain: A response to local subsidence (Miocene of the Duero basin, Spain).
20 *Sediment Geol*, **177**, 253-270.
- 21 HUERTA, P., ARMENTEROS, I., RECIO, C. & BLANCO, J.A. (2010). Palaeogroundwater evolution
22 in playa-lake environments. Sedimentary facies and stable isotope record
23 (Palaeogene, Almazán basin, Spain). *Palaeogeogr, Palaeoclimatol, Palaeoecol*, **286**,
24 135-148.
- 25 HUERTA, P., ARMENTEROS, I. & SILVA, P.G. (2011). Large-scale architecture in non-marine
26 basins: The response to the interplay between accommodation space and sediment
27 supply. *Sedimentology*, **58**, 1716-1736.
- 28 HUERTA, P. (2007). El Paleógeno de la cuenca de Almazán. Relleno de una cuenca piggyback.
29 PhD Thesis, Universidad de Salamanca, Salamanca, Spain.
- 30 JI, J., LUO, P., WHITE, P., JIANG, H., GAO, L., DING, Z. (2008) Episodic uplift of the Tianshan
31 Mountains since the Late Oligocene constrained by magnetostratigraphy of the Jingou
32 River section, in the southern margin of the Junggar Basin, China. *J. Geophys Res.*, **113**,
33 B05102, doi:10.1029/2007JB005064
- 34 JOHNSON, N. M., SHEIKH, K. A., DAWSON-SAUNDERS, E., & MCRAE, L. E. (1988). The use of
35 magnetic-reversal time lines in stratigraphic analysis: A case study in measuring
36 variability in sedimentation rates. In: *New perspectives in basin analysis* (Ed.
37 Kleinspehn, K. L., & Paola, C.), pp. 189–200. Springer-Verlag, New York.
- 38 KIM, G., ALLEMAN, L.Y. & CHURCH, T.M. (2004). Accumulation records of radionuclides and
39 trace metals in two contrasting Delaware salt marshes. *Mar. Chem.*, **87**, 87-96.
- 40 KIRSCHVINK, J.L. (1980). The least-squares line and plane and the analysis of palaeomagnetic
41 data. *Geophys. J. Int.*, **62**, 699–718. doi:10.1111/j.1365-246X.1980.tb02601.x
- 42 LEGARRETA, L. & ULIANA, M.A. (1998). Anatomy of hinterland depositional sequences: Upper
43 Cretaceous fluvial strata, Neuquén basin, west-central Argentina. In: *Relative role of*
44 *Eustasy, Climate, Tectonism in Continental Rocks* (Ed. K.W. Shanley & P.J. McCabe).
45 *SEPM Spec. P.*, **59**, 83-92. Society of Economic Paleontologists and Mineralogists,
46 Tulsa, OK, USA.
- 47 LÓPEZ MARTÍNEZ, N., AGUSTÍ, J., CABRERA, L., CALVO, J.P., CIVIS, J., CORROCHANO, A., DAAMS, R., DÍAZ,
48 M., ELÍZAGA, E., HOYOS, M., MARTÍNEZ, J., MORALES, J., PORTERO, J., ROBLES, F., SANTISTEBAN,
49 C. & TORRES, T. (1987) Approach to the Spanish Continental Neogene Synthesis and
50 Paleoclimatic Interpretation. *Annales Instituti Geologici Publici Hungarici*, **70**, 383-391.
- 51 MACHETTE, M.N. (1985) Calcic soils of southwestern United States. In: Weide, D.L. (Ed.), *Soil*
52 *and Quaternary Geology of the Southwestern United States*. *Geol. S. Am. S.*, **203**, pp.
53 1221
54
55
56
57
58
59
60

- 1
2
3
4
5
6
7
8
9
10
11
12
13
14
15
16
17
18
19
20
21
22
23
24
25
26
27
28
29
30
31
32
33
34
35
36
37
38
39
40
41
42
43
44
45
46
47
48
49
50
51
52
53
54
55
56
57
58
59
60
- MACKEY, S.D. & BRIDGE, J.S. (1995). Three-dimensional model of alluvial stratigraphy: theory and application. *J. Sediment. Res.*, **B65**, 7-31.
- MIALL, A.D. (2014) *Fluvial Depositional Systems*. Springer, New York, USA
- MICHAEL, N.A., WHITTAKER, A.C., CARTER, A. & ALLEN, P.A. (2014). Volumetric budget and grain-size fractionation of a geological sediment routing system: Eocene Escanilla Formation, south-central Pyrenees. *Geol. Soc. Am. Bull.*, **126**, 585-599.
- MITCHUM, R.M., JR., VAIL, P.R. & THOMPSON, S., III. (1977). Seismic stratigraphy and global changes of sea level. Part 2: The depositional sequence as a basic unit for stratigraphic analysis. In: *Seismic Stratigraphy; applications to Hydrocarbon Exploration* (Ed. C.E. Payton), *AAPG Mem.*, **26**, 53-62. American Association of Petroleum Geologists, Tulsa, OK.
- MUÑOZ-JIMÉNEZ, A. & CASAS-SAINZ, A.M. (1997) The Rioja Trough (N Spain): Tectosedimentary Evolution of a Symmetric Foreland Basin. *Basin Research*, **9**, 65-85.
- MUTO, T., & STEEL, R. J. (1997) Principles of regression and transgression: the nature of the interplay between accommodation and sediment supply. *J. Sedimen. Res.*, **67**, 994-1000.
- MUTO, T. & STEEL, R.J., (2000) The accommodation concept in sequence stratigraphy: some dimensional problems and possible redefinition. *Sediment. Geol.*, **130**, 1-10.
- NAVARRO VÁQUEZ, D. (1991). Mapa Geológico de España 1:50000, Hoja 350 (Soria), ITGE. Madrid.
- PAOLA, C. & MARTIN, J.M. (2012). Mass-balance effects in depositional systems. *J. Sediment. Res.*, **82**, 435-450.
- POSAMENTIER, H.W. & VAIL, P.R. (1988). Eustatic controls on clastic deposition. II: Sequence and systems tract models. In: *Sea-Level Changes-An Integrated Approach* (Ed. by C.K. Wilgus, B.S. Hastings, C. St. C. Kendall, H.W. Posamentier, C.A. Ross & J.C. Van Wagoner). *SEPM*, **42**, pp. 125-154. OK, USA
- ROSENBAUM, G., LISTER, G.S. & DUBOZ, C., (2002). Relative motions of Africa, Iberia and Europe during Alpine orogeny. *Tectonophysics* 359, 117–129. doi:10.1016/S0040-1951(02)00442-0
- SHANLEY, K.W. & MCCABE, P.J. (1991). Predicting facies architecture through sequence stratigraphy -an example from the Kaiparowits Plateau, Utah. *Geology*, **19**, 742-745.
- SHANLEY, K.W. & MCCABE, P.J. (1993). Alluvial architecture in a sequence stratigraphic framework: a case history from the Upper Cretaceous of southern Utah, USA. In: *Quantitative Description and Modelling of Clastic Hydrocarbon Reservoirs and Outcrop Analogues* (Ed. by S. Flint & I.D. Bryant). *Int. As. Sed.*, **15**, pp. 21–56.
- SHEETS, B.A., HICKSON, T.A. & PAOLA, C. (2002). Assembling the stratigraphic record: depositional patterns and time-scales in an experimental alluvial basin. *Basin Res.*, **14**, 287-301.
- STRONG, N., SHEETS, B.A., HICKSON, T.A. & PAOLA, C. (2005). A mass-balance framework for quantifying downstream changes in fluvial architecture. In: *Fluvial Sedimentology VII*. (Ed. M.D. Blum, S.B. Marriott & S. Leclair), *Int. As. Sed.*, **35**, pp. 243-253. Blackwell.
- TANDON, S.K., ANDREWS, J.E., SOOD, A. & MITTAL, S. (1998) Shrinkage and Sediment Supply Control on Multiple Calcrete Profile Development: A Case Study from the Maastrichtian of Central India. *Sediment. Geol.*, **119**, 25-45.
- TÖRNQVIST, T.E. (1994) Middle and late Holocene avulsion history of the River Rhine (Rhine-Meuse delta, Netherlands). *Geology*, **22**, 711-714.
- VAIL, P.R. & MITCHUM, R.M., JR. (1977). Seismic Stratigraphy and global changes of sea level. Part 1: Overview. In: *Seismic Stratigraphy - Applications to Hydrocarbon Exploration*, (Ed. by C.E. Payton). *AAPG Mem.*, **26**, 51-52. American Association of Petroleum Geologists, Tulsa, OK.

- 1
2
3 VALERO, L., GARCÉS, M., CABRERA, L., COSTA, E., & SÁEZ, A. (2014). 20 Myr of eccentricity
4 paced lacustrine cycles in the Cenozoic Ebro Basin. *Earth Planet. Sci. Lett.*, **408**, 183-
5 193.
- 6 VAN WAGONER, J.C., POSAMENTIER, H.W., MITCHUM, R.M., JR., VAIL, P.R., SARG, J.F., LOUTIT,
7 T.S. AND HARDENBOL, J. (1988). An overview of the fundamentals of sequence
8 stratigraphy and key definitions. In: *Sea-Level Changes-An Integrated Approach* (Ed. by
9 C.K. Wilgus, B.S Hastings, C. St. C. Kendall, H.W. Posamentier, C.A. Ross & J.C. Van
10 Wagoner). *SEPM*, **42**, pp. 39-45. OK, USA.
- 11 WRIGHT, V.P. & MARRIOTT, S.B. (1993). The sequence stratigraphy of fluvial depositional
12 systems: the role of floodplain sediment storage. *Sediment. Geol.*, **86**, 203-210.
13
14
15
16
17
18
19
20
21
22
23
24
25
26
27
28
29
30
31
32
33
34
35
36
37
38
39
40
41
42
43
44
45
46
47
48
49
50
51
52
53
54
55
56
57
58
59
60

Table 1

Channel density values for eight boxes of the Gómara Monocline. 4 in DS A2 and 4 in DS A3. The exact location of the Boxes can be found in a supplementary file (.kmz)

Table 2.

Sedimentation rates values for different intervals within the Gómara Monocline.

Figure 1

a) Tectonic map of the Northeastern domain of the Almazán basin, where the depositional sequences are shown, after Huerta et al., (2011). The main tectonic structures are also indicated. Squared in the center is indicated the location of Fig. 2. B) Cross section oriented SSE-NNW, which location is shown above at the left. The depositional sequences and the tectonic domains of the basin are indicated.

Figure 2

Detailed map of the lithostratigraphic formations cropping out along the Gómara monocline (see location in Fig. 1). In grey, the trace of fluvial channels is marked. Dark green line shows the magnetostratigraphic sampling track.

Figure 3

Field photographs of the main large-scale architectural elements identified in the Paleogene succession of the Almazán Basin. A) Low interconnected ribbon-shaped channel fills (Alparrache Formation). B) Highly interconnected sheet-like channel fills (Upper part of the Gómara Formation). C) and D) shallow water lacustrine carbonates of the Deza Formation, D) an almost complete view of the carbonate deposits (about 200 m) is shown. E) Mudflat deposits of the Bordalba Formation (close to the Colmenares section). F) Stacked calcretes at the base of the Mazaterón Formation, which top is at the right of the picture.

Figure 4

Changes in the interconnectivity of channels due to variations in fluvial regime are recorded several times in the Gómara Formation. A) Example of low-density of fluvial channels areas, which mainly bear ribbon-like channel fills with low W/T ratios. B) High density of channels. Sheet-like channel fills, with high W/T ratios. In this case, located in the top of A3, W/T ratios overcome 100.

Figure 5

A) Stepwise NRM thermal demagnetization (Zijderveld plots) of representative lithologies and normalized NRM and magnetic susceptibility changes upon heating from the Almazul and Mazaterón sections. M0: Initial NRM in 10^{-6} A/m. B) Stereographic projection of the ChRM directions before and after tectonic correction and their associated normal and reversed mean directions by means of Fisherian statistics.

1
2
3 Figure 6

4
5 Local litho- and magnetostratigraphic composite section. From left to right, changes in
6 declination, inclination and Virtual Geomagnetic Pole (VGP) paleolatitudes. The correlation
7 between Almazul and Mazaterón sections was performed by means of magnetostratigraphy.
8 Stable magnetozones were defined by at least two adjacent palaeomagnetic sites of the same
9 polarity. Normal magnetozones are represented in black and reversed magnetozones are
10 represented in white. Single site reversals are represented by half bar magnetozones
11

12
13 Figure 7.

14
15 Correlation between the local magnetostratigraphic section of Almazán to the GPTS (Gradstein
16 *et al.*, 2012), including the formations and the depositional sequences of the Almazán basin.
17 The red line indicates the location of Miñana fossil site and its correlation to the GPTS.
18
19

20 Figure 8

21
22 Magnetostratigraphic map of the Gómara monocline. Magnetic reversals had been extended
23 through the monocline following traceable levels. Black bands mark the normal magnetic
24 polarity intervals. The magnetostratigraphic sampling track has been marked and corresponds
25 to the Almazul and Mazaterón sections, unified as Miñana transect in this figure. The other
26 sections shown correspond to the ones where sedimentation rates were calculated (Fig. 9).
27 Geological formations are included. A widening of the magnetic reversals towards the NW,
28 where clastic formations dominate can be distinguished.
29
30

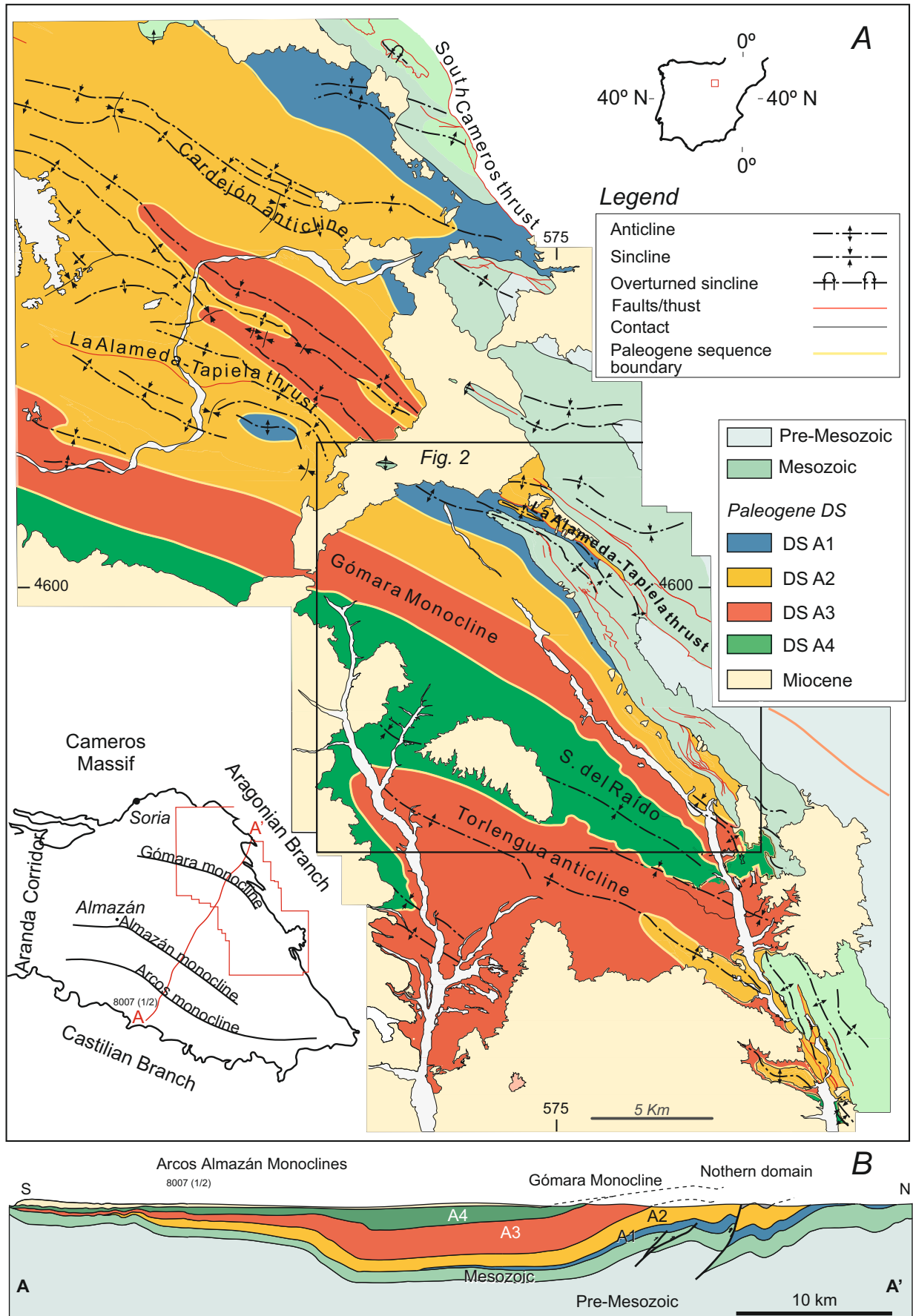
31 Figure 9

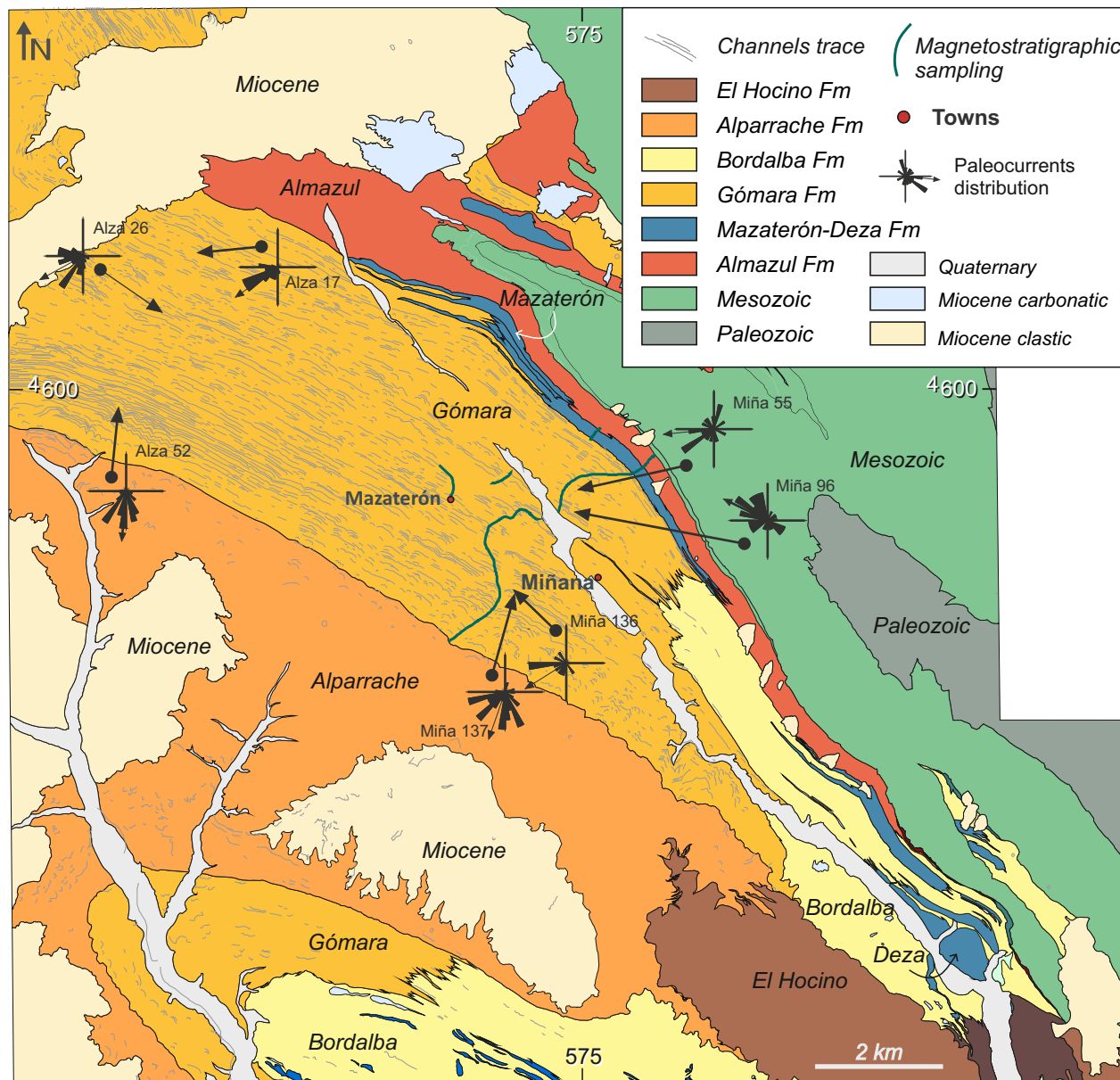
32
33 Sedimentation rates resulting from plotting stratigraphic thicknesses against
34 magnetostratigraphic ages for 4 key transects (location in Fig. 8). These sections encompass
35 the most characteristic formations and large-scale architectures of the Almazán Basin.
36 Polygons indicate the sedimentary environments, which nearly coincide with the formations.
37 The stacking pattern is drawn in circles, and its perimeter color indicates the section. The
38 numbers refer to Sedimentation Rates, (in cm/kyr), and are calculated within magnetic
39 reversals, which are the vertical underlying white or grey stripes. Each section has its own
40 thickness coordinates origin, only for representative purposes.
41
42
43

44 Figure 10

45
46 Summary of the evolution of tectonic uplift and subsidence for the four Paleogene tectonic
47 domains during the four depositional sequences (right). Subsidence and uplift are estimated
48 from the architectural arrangement. The syn-sedimentary styles and the development of
49 alluvial fans as consequence of the uplift of nearby structures are shown. MCT, Main Cameros
50 Thrust; SCT, South Cameros Thrust; C A/T, Cardejón Anticline/Thrust; ATT, La Alameda-Tapiela
51 Thrust; GM, Gómara Monocline; TA, Torlengua Anticline; AAM, Almazán-Arcos Monoclines
52 (see Fig.1 for location).
53
54
55
56
57
58
59
60

1
2
3
4
5
6
7
8
9
10
11
12
13
14
15
16
17
18
19
20
21
22
23
24
25
26
27
28
29
30
31
32
33
34
35
36
37
38
39
40
41
42
43
44
45
46
47
48
49
50
51
52
53
54
55
56
57
58
59
60

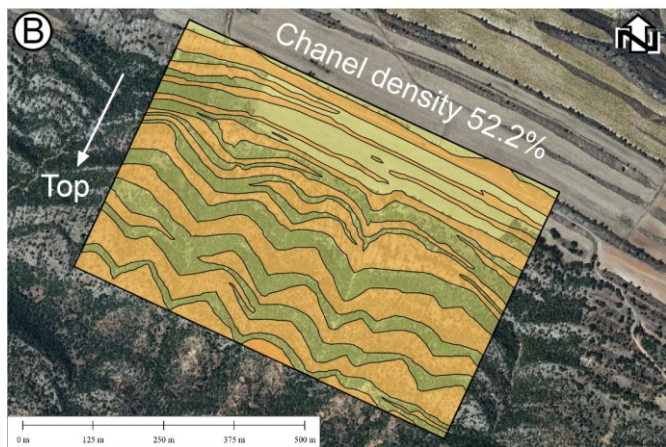
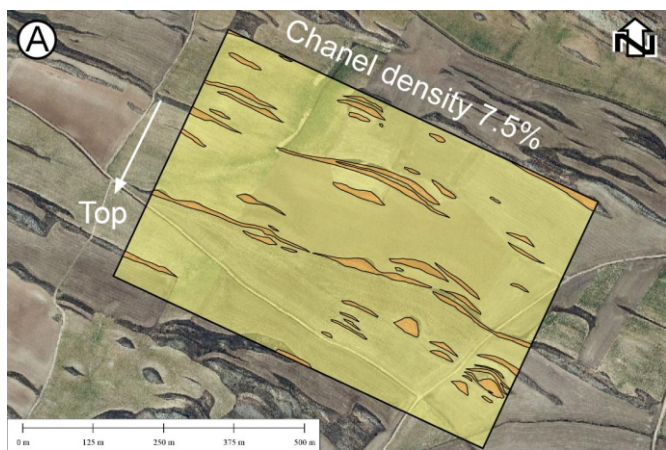




1
2
3
4
5
6
7
8
9
10
11
12
13
14
15
16
17
18
19
20
21
22
23
24
25
26
27
28
29
30
31
32
33
34
35
36
37
38
39
40
41
42
43
44
45
46
47
48
49
50
51
52
53
54
55
56
57
58
59
60

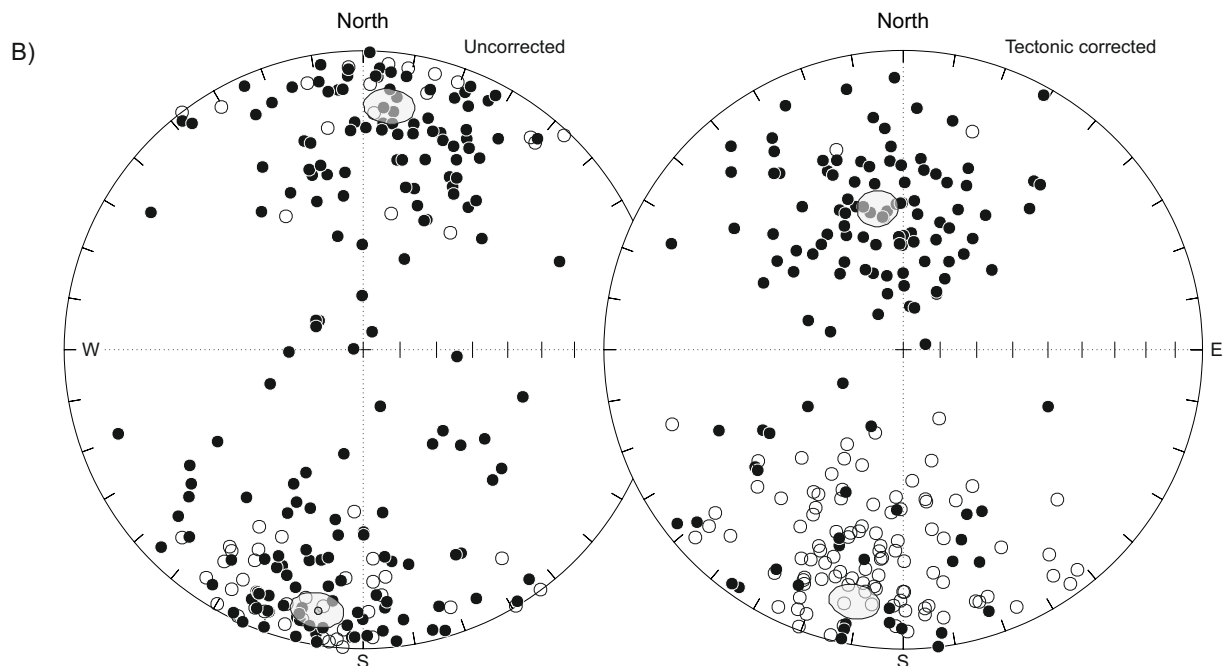
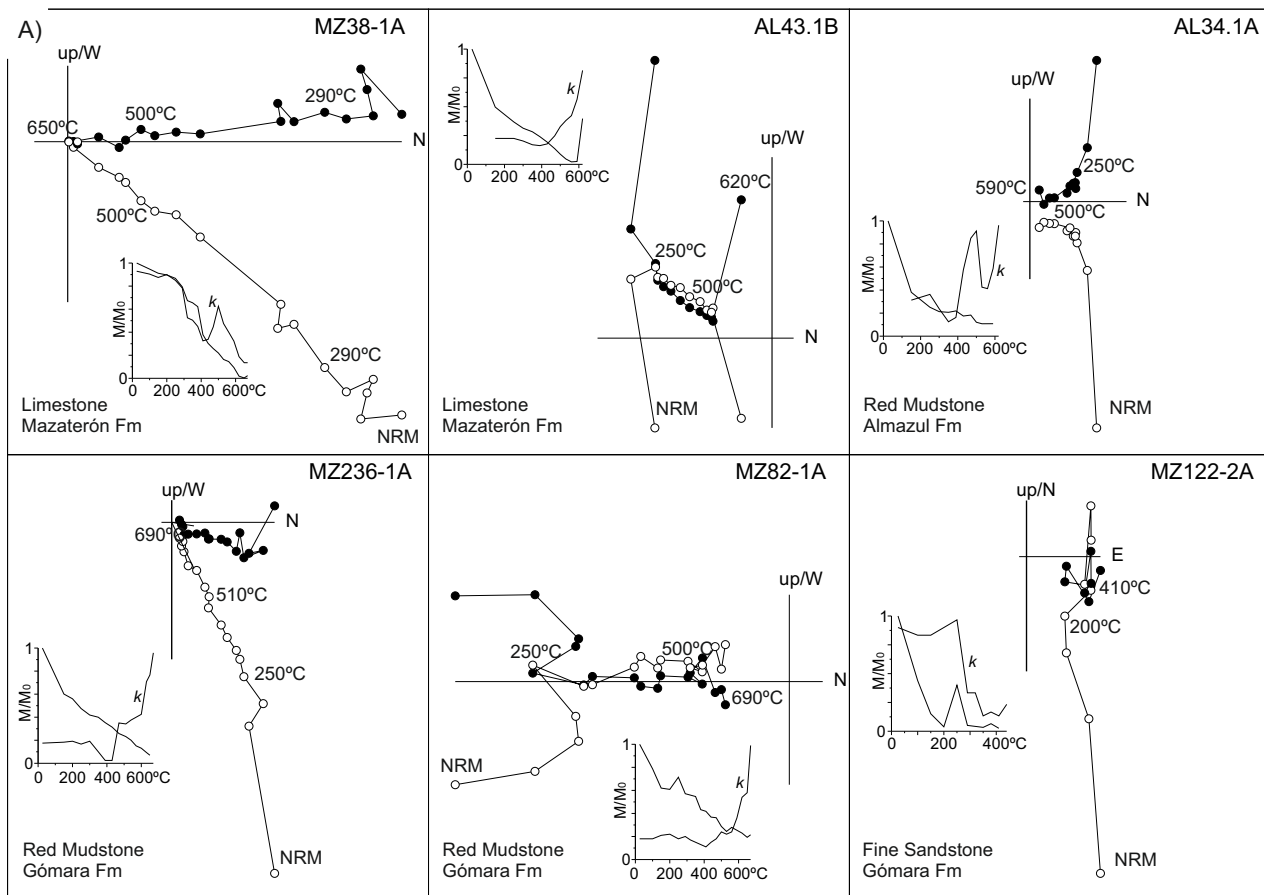


1
2
3
4
5
6
7
8
9
10
11
12
13
14
15
16
17
18
19
20
21
22
23
24
25
26
27
28
29
30
31
32
33
34
35
36
37
38
39
40
41
42
43
44
45
46
47
48
49
50
51
52
53
54
55
56
57
58
59
60

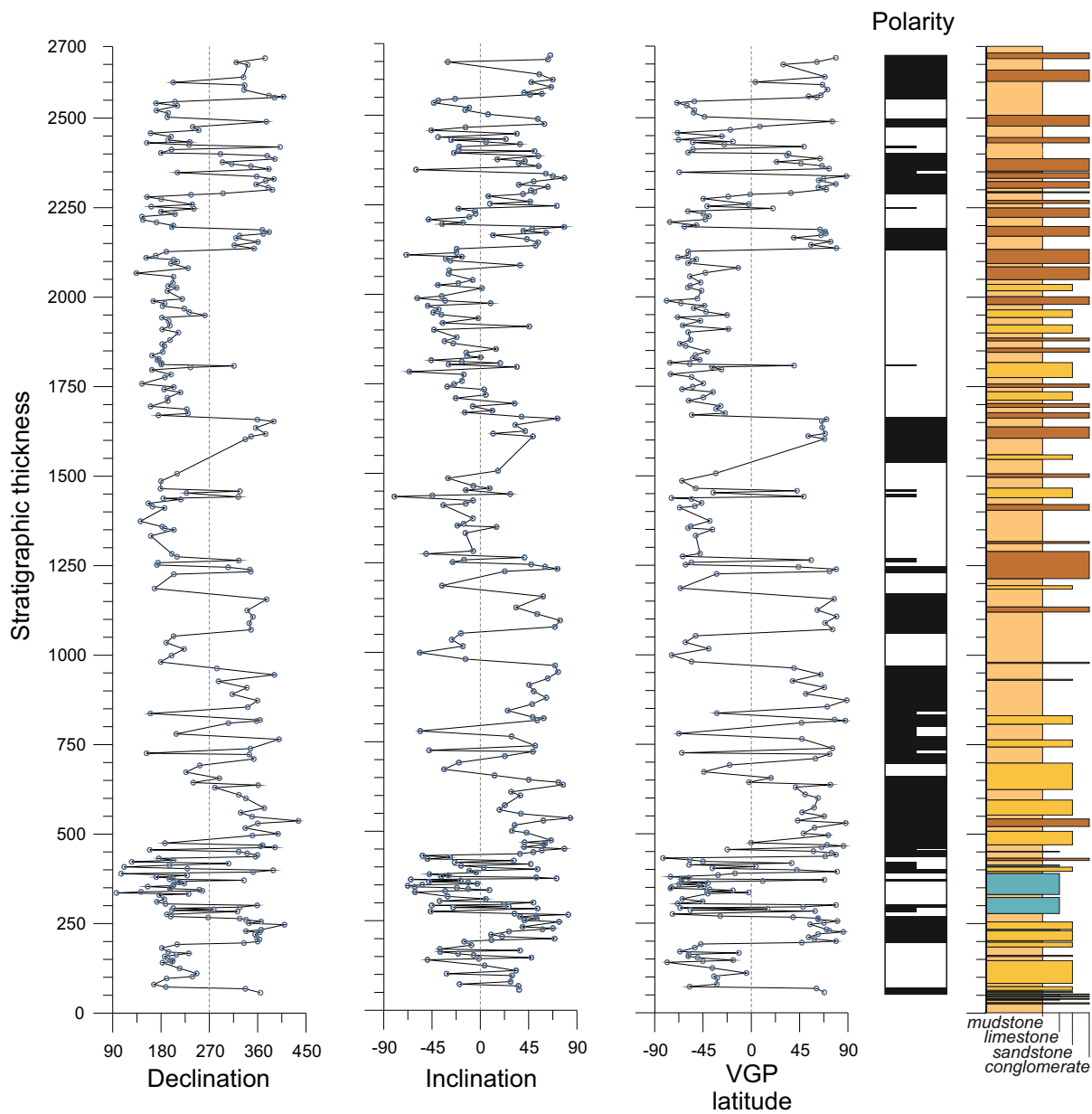


Dimensions		Middle-scale channel architecture
width	W/T	
1.5 - 50 m	3:1 to 15:1	<p>Ribbon-shaped bodies</p> <p>Vertical stacking</p> <p>Lateral expansion wings</p> <p>Dominated by conglomerates and sandstones</p>
50 - 500 m	25:1 to 50:1	<p>Intermediate sheet-like bodies</p> <p>Dominated by lenticular bodies</p> <p>Dominated by lateral accretions</p> <p>Gentle dipping lateral accretions</p> <p>Multi-storey fills</p> <p>Dominated by coarse sandstone and mixed</p>
> 500 m	> 100:1	<p>Sheet-like channel bodies</p> <p>Dominated by conglomerates</p>

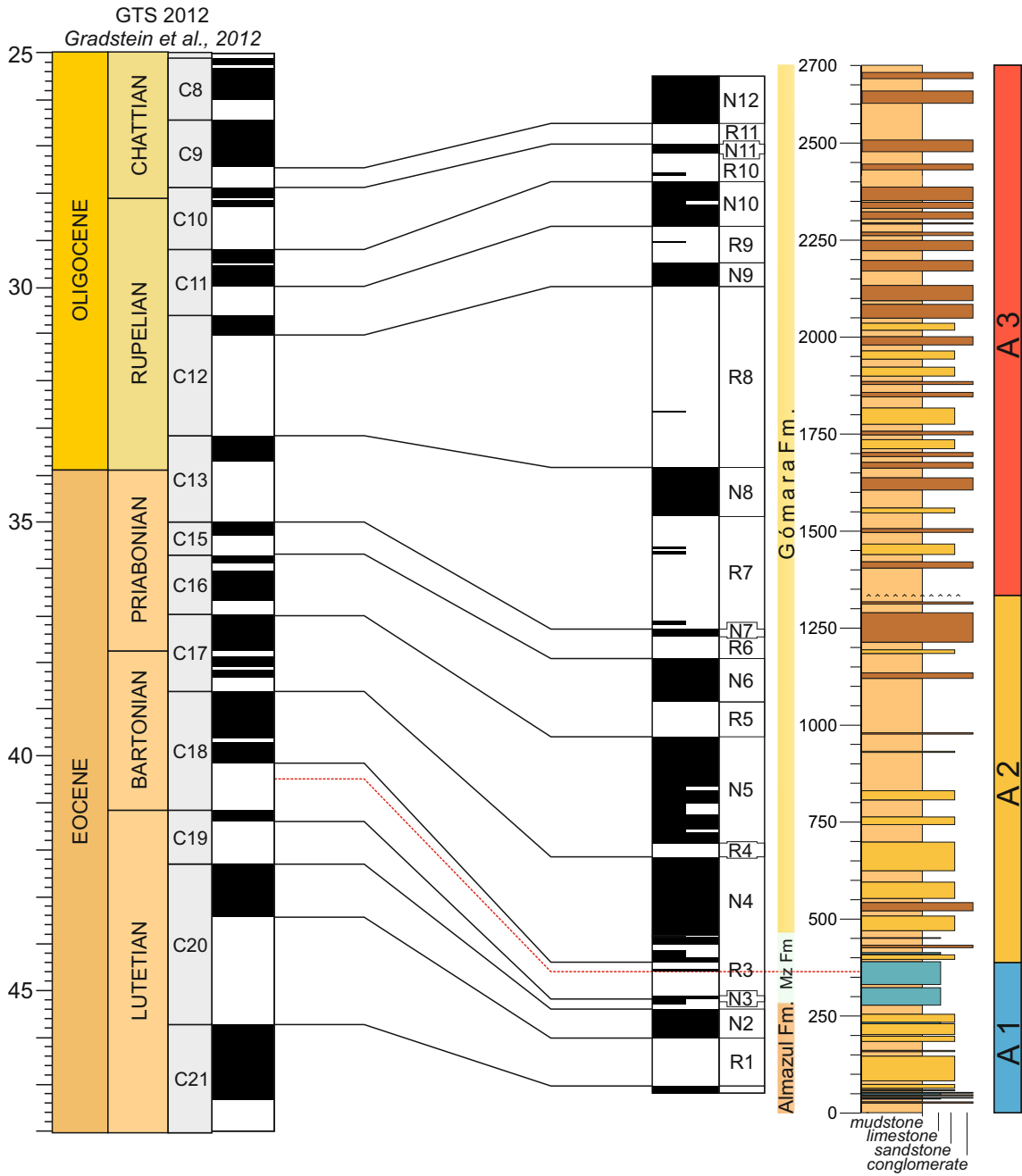
1
2
3
4
5
6
7
8
9
10
11
12
13
14
15
16
17
18
19
20
21
22
23
24
25
26
27
28
29
30
31
32
33
34
35
36
37
38
39
40
41
42
43
44
45
46
47
48
49
50
51
52
53
54
55
56
57
58
59
60

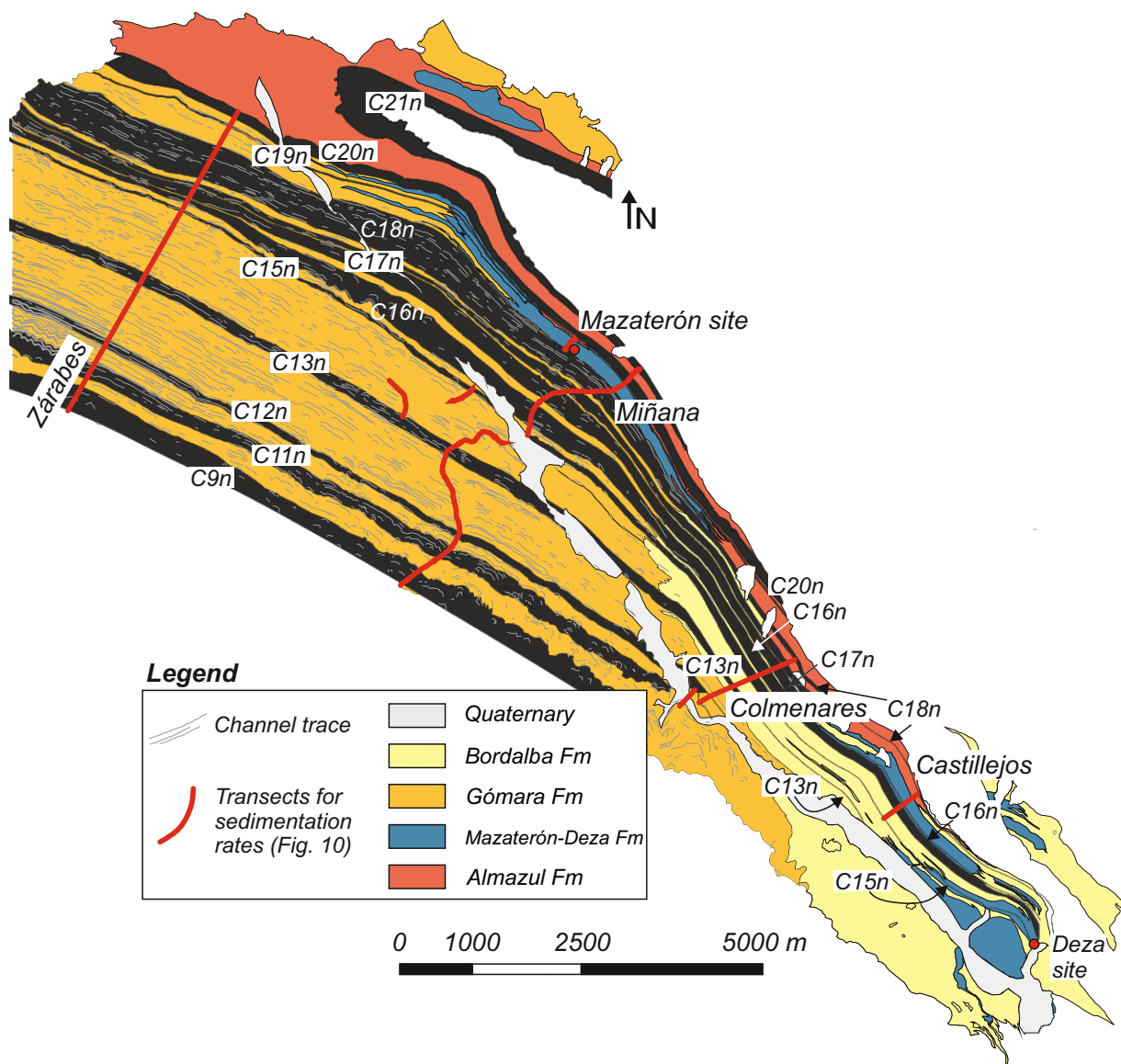


Polarity	Uncorrected					Tectonic corrected				
	N	Dec	Inc	Ks	α_{95}	N	Dec	Inc	Ks	α_{95}
Normal	104	6.3	21.2	7.1	5.6	104	349.9	50.8	8.3	5.1
Reverse	130	190.0	15.0	5.7	5.7	130	191.0	-18.1	6.1	5.5

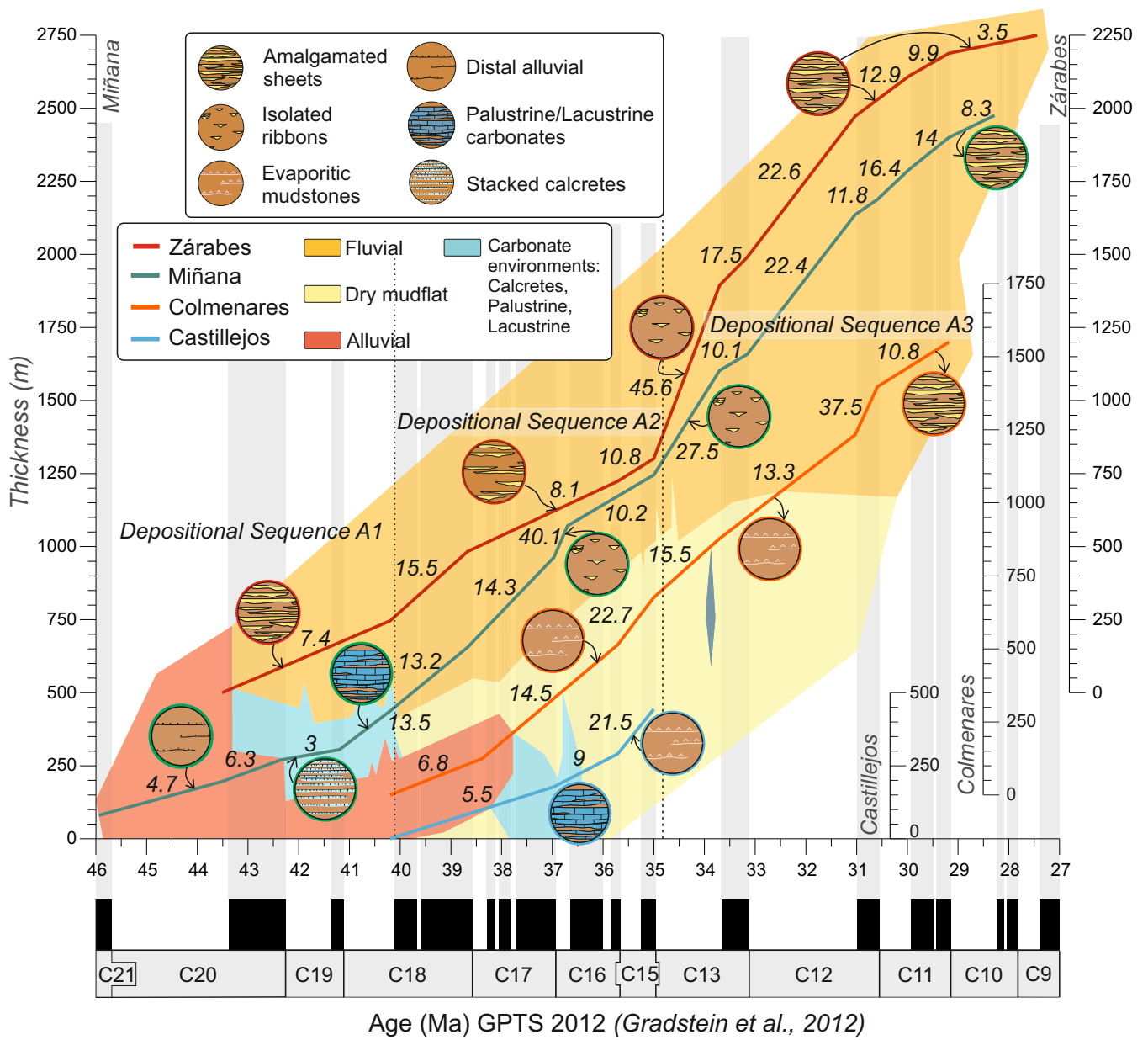


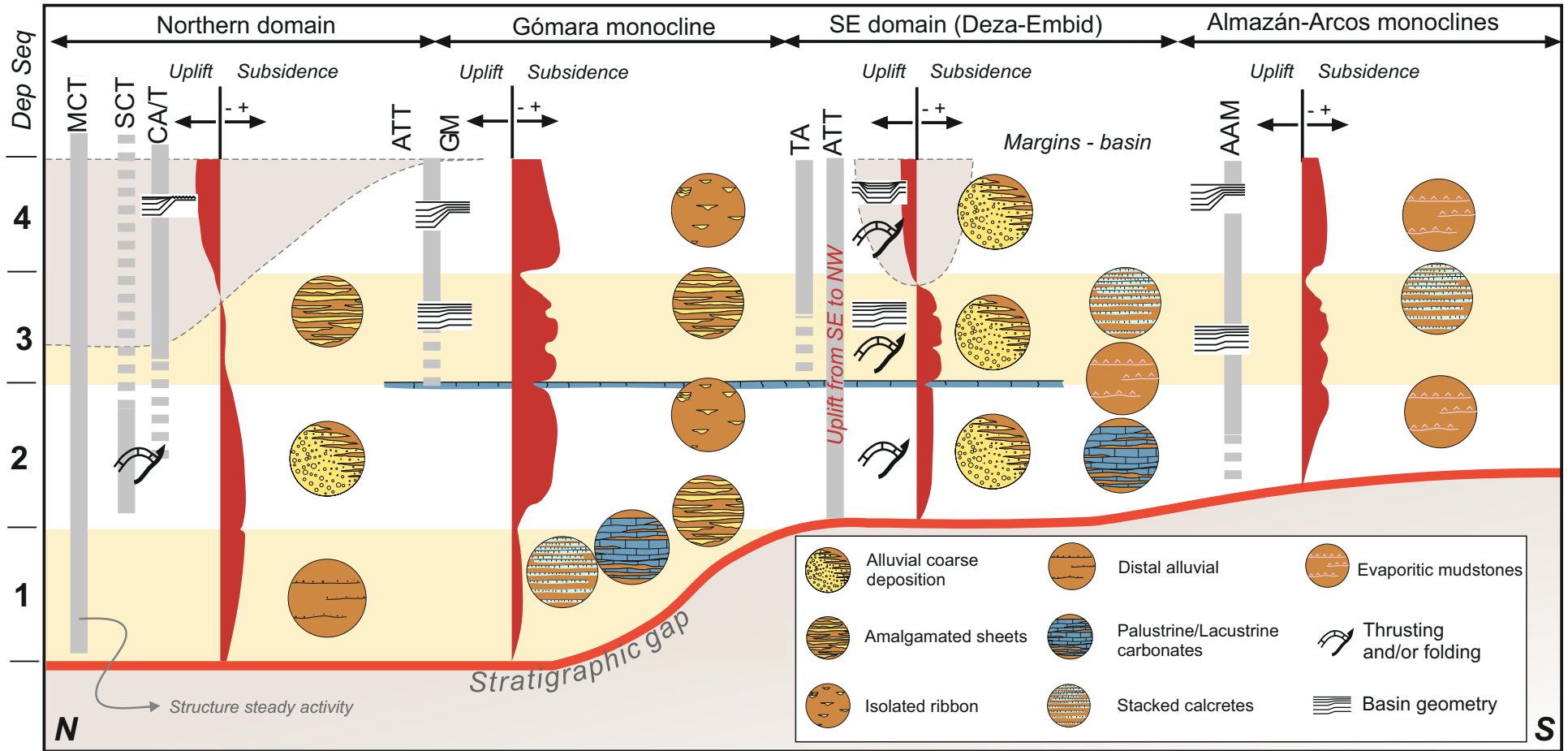
1
2
3
4
5
6
7
8
9
10
11
12
13
14
15
16
17
18
19
20
21
22
23
24
25
26
27
28
29
30
31
32
33
34
35
36
37
38
39
40
41
42
43
44
45
46
47
48
49
50
51
52
53
54
55
56
57
58
59
60





1
2
3
4
5
6
7
8
9
10
11
12
13
14
15
16
17
18
19
20
21
22
23
24
25
26
27
28
29
30
31
32
33
34
35
36
37
38
39
40
41
42
43
44
45
46
47
48
49
50
51
52
53
54
55
56
57
58
59
60





1
2
3
4
5
6
7
8
9
10
11
12
13
14
15
16
17
18
19
20
21
22
23
24
25
26
27
28
29
30
31
32
33
34
35
36
37
38
39
40
41
42
43
44
45
46
47

1
2
3
4
5
6
7
8
9
10
11
12
13
14
15
16
17
18
19
20
21
22
23
24
25
26
27
28
29
30
31
32
33
34
35
36
37
38
39
40
41
42
43
44
45
46
47
48
49
50
51
52
53
54
55
56
57
58
59
60

# Box	Depositional sequence	Box area (km ²)	∑Channel fill area (km ²)	Channel density (%)
1	A2	0.35	0.020	5.64
2	A2	0.35	0.022	6.40
3	A2	0.35	0.026	7.52
4	A2	0.35	0.015	4.42
5	A3	0.35	0.155	44.40
6	A3	0.35	0.116	33.23
7	A3	0.35	0.183	52.22
8	A3	0.35	0.077	22.04

Table 1: Channel density calculated for 8 boxes. 4 in DS A2 and 4 in DS A3.

Zárabes section								
Interval	Initial Age (Ma)	Final Age (Ma)	Thickness increase (m)	Acummulated thickness (m)	Age increase (Ma)	Sedimentation rate (cm/kyr)	Dip direction	Dip
1	43.51	40.2	245.73	245.73	3.31	7.42	206	25
2	40.2	38.67	237.47	483.2	1.53	15.52	200	30
3	38.67	35.71	240.65	723.85	2.96	8.13	203	35
4	35.71	35	77.3	801.15	0.71	10.89	206	35
5	35	33.7	593.63	1394.78	1.3	45.66	206	35
6	33.7	33.16	94.96	1489.74	0.54	17.59	206	35
7	33.16	31.03	483.14	1972.88	2.13	22.68	208	30
8	31.03	29.97	137.44	2110.32	1.06	12.97	208	25
9	29.97	29.18	78.24	2188.56	0.79	9.90	209	20
10	29.18	27.44	61.58	2250.14	1.74	3.54	208	20
Colmenares section								
Interval	Initial Age (Ma)	Final Age (Ma)	Thickness increase (m)	Acummulated thickness (m)	Age increase (Ma)	Sedimentation rate (cm/kyr)	Dip direction	Dip
1	40.2	38.38	124.98	124.98	1.82	6.87	55	60
2	38.38	35.71	389.19	514.17	2.67	14.58	55	75
3	35.71	35	161.73	675.9	0.71	22.78	55	85
4	35	33.7	201.79	877.69	1.3	15.52	55	90
5	33.7	31.03	354.73	1232.42	2.67	13.29	233	82
6	31.03	30.59	164.99	1397.41	0.44	37.50	232	79
7	30.59	29.18	152.57	1549.98	1.41	10.82	232	45
Castillejos section								
Interval	Initial Age (Ma)	Final Age (Ma)	Thickness increase (m)	Acummulated thickness (m)	Age increase (Ma)	Sedimentation rate (cm/kyr)	Dip direction	Dip
1	40.2	36.97	177.54	177.54	3.23	5.50	233	61
2	36.97	35.71	113.23	290.77	1.26	8.99	233	61
3	35.71	35	152.75	443.52	0.71	21.51	233	61